Author(s): Kemppainen, Erno & Halme, Janne & Lund, Peter

Title: Physical Modeling of Photoelectrochemical Hydrogen Production Devices

Year: 2015

Version: Post print

Please cite the original version:

Kemppainen, Erno & Halme, Janne & Lund, Peter. 2015. Physical Modeling of Photoelectrochemical Hydrogen Production Devices. The Journal of Physical Chemistry C. Volume 119, Issue 38. 21747-21766. DOI: 10.1021/acs.jpcc.5b04764.

Physical Modeling of Photoelectrochemical Hydrogen Production Devices

Erno Kemppainen, Janne Halme*, Peter Lund

Aalto University School of Science, Department of Applied Physics, P.O.Box 15100, FI-00076

Aalto, Finland. E-mail: janne.halme@aalto.fi

Physical Modeling of Photoelectrochemical Hydrogen Production Devices

Abstract

Solar-powered water splitting with photoelectrochemical (PEC) devices is a promising method to simultaneously harvest and store solar energy at a large scale. Highly efficient small prototype PEC devices reported recently demonstrate a move from basic material research towards design and engineering of complete devices and systems. The increased interest in engineering calls for better understanding about the operational details of PEC devices at different length scales. The relevant physical phenomena and the properties of typical materials are well known for separate device components, but their interaction in a complete PEC cell has received less attention. Coupled physical models are useful for studying these interactions and understanding the device operation as a whole, and for optimizing the devices. We review the central physical processes in solar-powered water splitting cells and the physical models used in their theoretical simulations. Our focus is in particular on how different physical processes have been coupled together to construct device models, and how different electrode and device geometries have been taken into account in them. Reflecting on the literature we discuss future opportunities and challenges in the modeling of PEC cells.

1. Introduction

Earth receives about 10000 times as much energy from Sun as humankind consumes[1]. This makes solar energy the most abundant energy source. The electromagnetic radiation energy of sunlight can be converted to electricity with photovoltaics (PV) or to heat with solar heat collectors and concentrating solar power (CSP) systems. These energy conversion technologies are already mature and offer heat and electricity at prices comparable to burning fossil fuels[2].

However, there is one significant challenge for the widespread utilization of solar energy: storage. The local intensity of sunlight varies on the seasonal, daily and hourly basis, which means that generation of solar energy can temporarily exceed its consumption or fall behind it. Storing the surplus solar energy for later use to ensure a steady and controllable supply could solve this problem. Some heat storage methods are already mature and allow long-term storage of large amounts of energy [2]. On the contrary, it is difficult to store electricity economically at large quantities and for long time periods.

One of the studied methods is to use solar energy to produce fuels that would be easy to store and transport, similarly to fossil fuels. Unlike fossil fuels, solar fuels that are based on closed carbon cycle or contain no carbon at all do not produce net carbon dioxide emissions. The best-known solar fuel candidate for renewable energy infrastructure is hydrogen which is already produced in large quantities. However, almost all of its production is based on fossil fuels, the most significant production method being the steam reforming of methane[3,4]. Most of the produced hydrogen is used in chemical industry: Ammonia synthesis alone consumes globally 62% of the produced hydrogen, oil refineries 24% and methanol production about 9%[5]. Because those processes consume enormous amounts of hydrogen, it is typically also produced at the same facility that consumes it[5]. Hydrogen can also be used in fuel cells to generate electricity, but this does not make

a significant part of the overall hydrogen consumption yet although it offers higher efficiency than obtained in combustion processes.

Renewable hydrogen can be produced with the electrolysis of water, also known as water splitting. In solar powered electrolysis, the electric power required by the electrolyzer is produced with a PV system. However, these two functions, namely photovoltaic conversion and electrochemical reactions, can also be carried out in a single device, a photoelectrochemical (PEC) cell[6,7]. In a PEC cell, a semiconductor photoelectrode (PE) absorbs photons and generates charge carriers, electrons and holes, and separates them to electrodes, where they drive the hydrogen (HER) and oxygen evolution reactions (OER). Ionic transport in the electrolyte, the collection of hydrogen and oxygen, and continuous supply of water complete the cycle. Compared with a separate PV system and electrolyzer, an integrated single-unit photoelectrolysis cell can have a cost advantage since it uses fewer system components. On the other hand, integrating separate system functions into a single unit requires solving additional engineering design challenges to make the integrated parts work seamlessly together.

It has been estimated that PEC hydrogen production could become as cheap as steam reforming of methane, provided that the technological requirements are fulfilled[8]. As with the development of any energy conversion technology, the main challenge with PEC water splitting is to combine high efficiency with good stability and a reasonable price. Most of the research and development has been directed to the search and development of materials that could allow constructing a device that would satisfy all these three criteria simultaneously. Thus far the highest solar-to-hydrogen conversion efficiencies have been achieved with devices based on high-efficiency PV materials and separate electrodes[9–13].

While the search for more efficient and durable PE materials, catalysts and electrode architectures continues, research is moving gradually towards designing and testing complete PEC prototype devices. As the PEC technology approaches practical feasibility, it becomes increasingly important to understand how the material properties and device designs affect the overall system efficiency. An essential tool for this is mathematical modeling.

Going through the literature of PEC modeling, the following two basic observations can be made: First, the models cover a broad range of length scales, from the electronic structure calculations of catalyst surface carried out in the sub-atomic scale (e.g.[14,15]), to the hydrodynamic calculations of the circulating electrolyte in the scale to several centimeters[16]. Second, the mathematical methods and their computational costs differ substantially depending on the complexity of the phenomena and approximations made in managing it (e.g.[17–21]). This is understandable since, due to limited computational resources it is best to approach any research problem with a purposely limited mathematical model that is detailed enough to capture the essentials but simplified enough to omit unnecessary details. Nevertheless, to get an overall picture of the operation of a complete PEC device, one needs to understand not only the physics and electrochemistry of the individual device functions but also how they are connected to each other.

The purpose of this review is to give a broader overview of the modeling landscape of PEC devices, serving both the purpose of a tutorial text and a critical review of the most recent literature. In doing so, we emphasize in particular the interaction between different physical phenomena and modeling regimes. Understanding how the different aspects of the PEC device operation, such as light absorption, charge transport, interfacial reactions and mass transport are connected to each other is necessary for building complete device level models. In practice it requires solving simultaneously, or iteratively, equations describing the anode and cathode operation as well as the

transport of ions in the electrolyte. Evolution of hydrogen and oxygen at the electrodes further complicate the modeling problem, but are also important for the practical operation of the PEC devices.

We believe that illuminating the interdependencies between the microscopic phenomena of photoelectrolysis reactions, that have been the main subject of research thus far, and the macroscopic phenomena that are becoming increasingly important for designing complete PEC devices, could speed up the systematic progress towards complete prototype PEC devices. This overview is therefore aimed as a future guide to system level modeling of PEC devices.

The paper is organized as follows: First we give an overview to photoelectrochemical hydrogen production, including the most important phenomena and the structure of the devices. We also introduce a few recent prototypes to illustrate the current state of the art. After discussing the implications of the device structure on modeling we discuss modeling related to the main phenomena of the devices (light absorption, charge transport and kinetics of the electrochemical reactions) before taking a look at the modeling of complete devices.

2. Photoelectrochemical Water Splitting

At a general level, the operating principle of PEC hydrogen production appears simple: Convert solar irradiation to electricity and use it to drive water electrolysis. The net result of the process is the production of hydrogen and oxygen from water, which is typically used as a strongly acidic or basic electrolyte solution to minimize voltage losses. The total reaction consists of two half reactions: the hydrogen evolution reaction (HER) and the oxygen evolution reaction (OER). Driving these reactions requires a voltage that a semiconductor produces from sunlight via PV operation.

2.1. Operating Principle

The first process in the chain that converts sunlight and water to hydrogen (and oxygen) is *light absorption* (1 in Figure 1). The fraction of the incident light that leads to the generation of charge carriers depends most on the optical properties of the absorber material, but is also affected by the other cell components and the device design that can cause optical losses due to parasitic absorption or reflection losses. There are also a range of optical management techniques used to enhance light absorption, for instance plasmonic nanoparticles and resonance (constructive interference) in thin films[22,23].

The absorbed photons excite electrons to higher energy states, in semiconductors from the valence band (VB) to the conduction band (CB), creating an electron-hole-pair in the photoanode (1 in Figure 1). The holes that reach the electrolyte interface (2) drive the oxygen evolution reaction (OER) at the anode (3), whereas the electrons that reach the electrode substrate are extracted to the external electrical circuit and are used to drive the hydrogen evolution reaction (HER) at the cathode (4). The electron - hole pair can recombine either in the bulk of the semiconductor or at the electrolyte interface for example via reaction intermediates (5), which are loss mechanisms that reduce the efficiency of the device. The operating cycle of the system is completed by ionic transport in an electrolyte solution between the electrodes (6), and by a continuous supply of liquid water (7) and removal of gaseous hydrogen and oxygen (8).

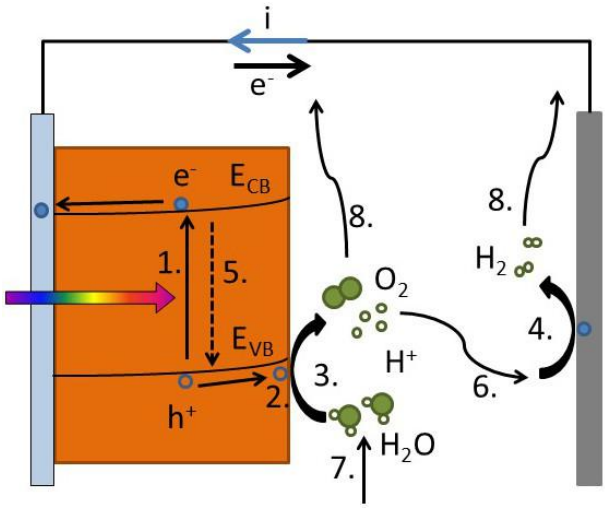

Figure 1. Illustration of the processes in a PE of a water splitting device (photoanode in acidic electrolyte, reactions 3 and 4 on electrodes are not placed on energy/potential scale with CB and VB level).

2.2. PEC Device Structures

Combining PV operation and electrochemistry together in a single integrated device can be accomplished in several ways. One way to organize the PEC device structures reported in the literature is to categorize them according to the details of their physical operating principles[24]. Another way to look at the range of device architectures is to consider them as a step-wise transition between a tightly integrated PEC cell and a fully separate PV and electrolyzer, as illustrated recently by Jacobsson et al. (Figure 2) [7]. We use the latter categorization as a framework for the discussions in the present paper.

In the PEC cells, all functions of the device are integrated into a single, more or less tightly packed unit that performs both the solar light absorption and the water splitting reactions. This eliminates the need for additional electrical components between the solar panels and the electrolyzer, but at the same time it increases the demands for chemical and functional compatibility related to

interfaces between materials[7]. At one end, we have devices built simply by connecting solar cells electrically to a separate water electrolysis cell (f in Figure 2). In fact, it is these types of devices, where the generation of photovoltage and the electrochemistry run by it are almost completely decoupled from each other, that have given the highest solar to hydrogen efficiencies among all PEC systems [7,25]. However, a device modeling study by Haussener et al. indicated that a more integrated, optimized PEC device (a in Figure 2) could produce in real operating conditions more hydrogen per year than a corresponding PV-powered electrolyzer system (g in Figure 2) [26]. The most significant advantage of the integrated system is the lack of a power converter between the light absorber and electrolyzer. Additionally, the integration of the photoabsorber to electrodes means that increase in operating temperature reduces kinetic and mass transport losses in the device[26]. This coupling might also operate "backwards" so that the electrolyte cools the photoabsorber, increasing its efficiency.

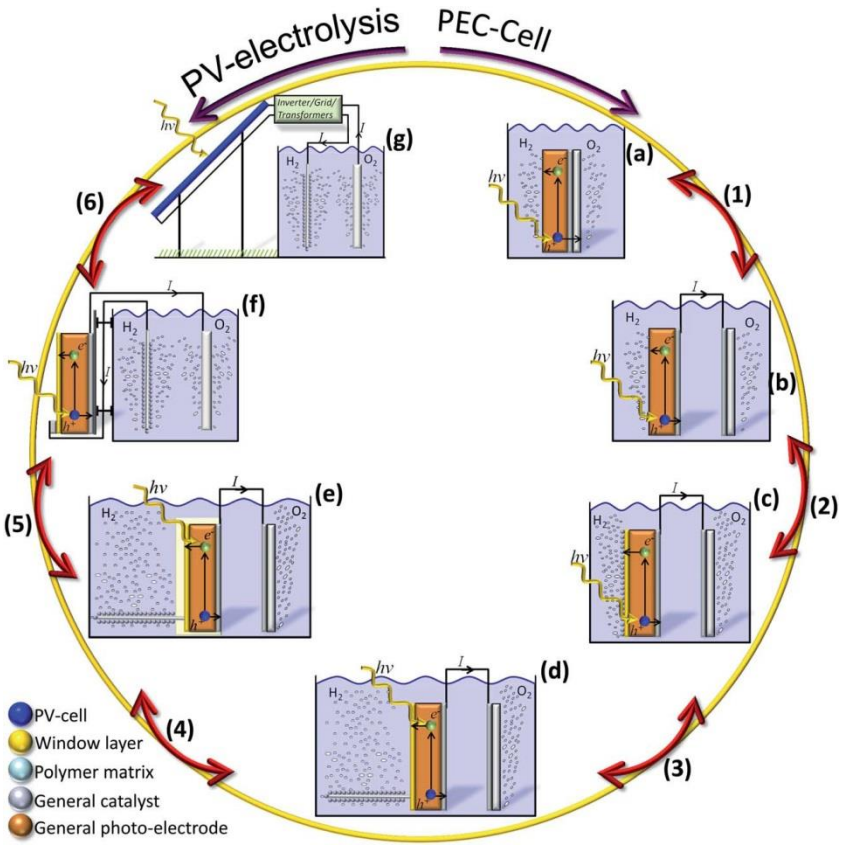

Figure 2. Illustration of a gradual transition in six steps from a monolithic device (a), to a free standing electrolyzer connected to PV-cell through a grid. Reproduced from Ref. [7] with permission from The Royal Society of Chemistry.

2.3. PEC Cell Prototypes

The TiO_2 PE reported in 1972 by Fujishima and Honda[27] is often considered the starting point for the research of PEC hydrogen production. Both the materials and devices have developed greatly since then. As an example, we consider in the following four more or less complete PEC device prototypes presented in the literature recently, which will serve as a practical background for the more theoretical discussions in this paper.

The first example is a PEC device based on a tandem microwire PE capable of unassisted water splitting demonstrated recently by Shaner et al. [28]. The wires consisted of a radial Si np^+-junction in an ohmic contact with WO_3 photocatalyst provided by an ITO layer between the two materials (Figure 3Figure 3). The main difference to the photocatalytic TiO_2 electrode of Fujishima and Honda[27] is that in this case, in addition to the semiconductor-liquid junction, the PE contains a pn junction that produces part of the photovoltage. In the Si microwires transport of holes takes place along the wires whereas electrons are collected radially across the np^+-junction. Ions and the evolving O_2 move in the electrolyte that fills the gaps between the wires. The device required concentrated illumination (10 suns, AM1.5D) for unassisted operation, and even then its efficiency was less than 0.01 %. It is nevertheless a proof of concept for the operation of a microstructured integrated tandem device. Several aspects of its operation could be improved to achieve higher hydrogen production rates, such as the OER catalyst.

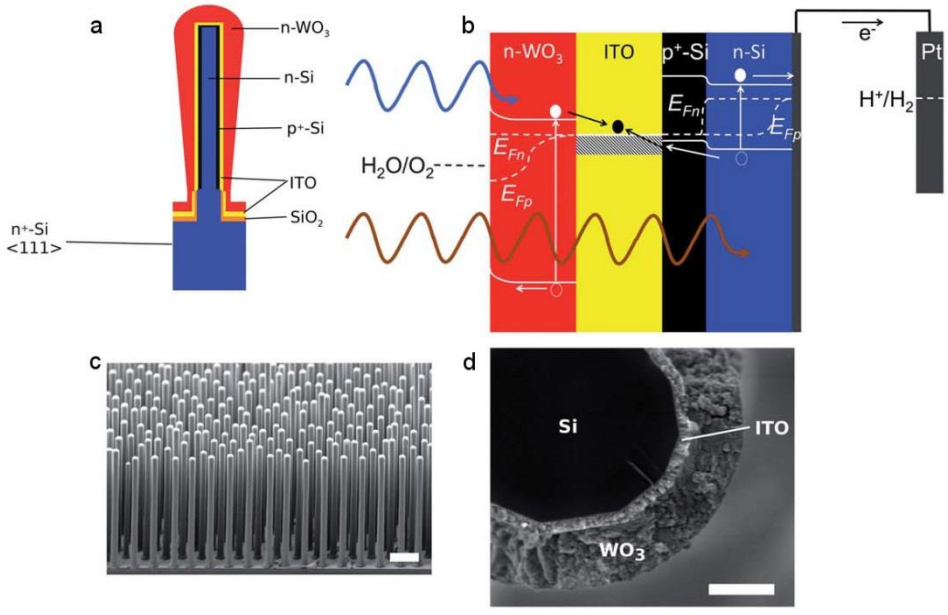

Figure 3. a) Scheme of the tandem junction microwire device b) energy level diagram of the device under illumination c) fully assembled tandem junction device array SEM (scale bar

= 10 μm) d) cross-sectional SEM of a fully assembled tandem junction single wire (scale bar = 500 nm) Adapted from Ref. [28] with permission from The Royal Society of Chemistry.

Another way of configuring a PEC cell is to separate the catalyst from the light absorber, while keeping them still immersed in the same electrolyte solution. A recent example of this is the CIGS-based monolithic device prototype by Jacobsson et al.[12]. Their device consisted of Pt sheet electrodes attached to three series-connected CIGS PV-cells that produced the operating voltage (Figure 4). One advantage of CIGS as a photoabsorber is that its bandgap can be tuned, and therefore optimized for solar hydrogen production[12]. However, due to the instability of CIGS in the electrolyte, the PV cells had to be covered with transparent protective coating. Because the electrodes were not integrated into the surface of the PV cells, the coating needed not to be electrically conductive but epoxy and polymers could be used as a protective coating. In PV operation, the efficiency of the CIGS solar cells was as high as 17%, but when coupled directly to the Pt electrodes to drive the HER and OER reactions, the solar to hydrogen efficiency was reduced to 10.5% mainly due to electrode overpotentials. Compared with the above-mentioned microwire electrode (Figure 3), the key difference of this device design is that the catalyst and the photoactive cells are not overlaid with each other, which simplifies both their practical integration and mathematical modeling. Nevertheless, being immersed in the same liquid medium as a single unit, the PV cells and the electrodes are not, strictly speaking, entirely independent operationally as the gas bubbles evolving at the electrodes can affect the PV cells by scattering part of the incident light (see Figure 4).

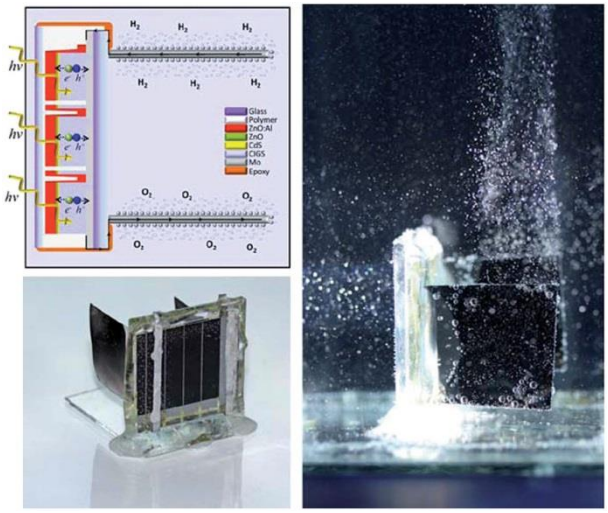

Figure 4. Top left: Sketch of the monolithic PV/PEC configuration seen from above. Bottom left: photo of the device Right: photo of the device in action. Adapted from Ref.[12] with permission from The Royal Society of Chemistry.

A further operational simplification is to place the solar cells entirely outside the electrochemical cell, connecting them together with external electric wires. A recent example of this comes from Luo et al.[13] who used two series connected methylammonium lead halide perovskite ($CH_3NH_3PbI_3$) solar cells to drive a separate electrolysis cell. Separating the PV and electrolysis units is a simple way to circumvent the incompatibility of the PV material with the electrolyte environment, such as with this perovskite material that is soluble to water [29]. On the one hand, this configuration can be considered simply as electrolysis of water using solar cells, but on the other hand, it could still be considered an integrated system, since no additional power conditioning such as DC/DC conversion and maximum power-point tracking were used. In this case, the current – voltage curves of the electrolysis and PV cells matched better with each other than in the case of the abovementioned CIGS-device, which allowed Luo et al. to reach higher solar-to-hydrogen efficiency (12.3%), even though their PV efficiency was lower (15.7%)[12,13]. From the point-of-

view of device modeling, the PV and electrolysis cells could in this case be modelled independently. Only their common operating voltage and current would be determined by the intersection of their individual current-voltage curves.

An example of a further step towards fully separate photovoltaic and electrolysis systems is the so-called HyCon cell [25,30] of Fraunhofer Institute for Solar Energy which is based on a concentrating PV cell and PEM electrolyzer stacked together. Compared with the other examples discussed above, the electrolyzer in the HyCon cell was more advanced as it included a gas separating membrane and flow field plates to improve electrolyte circulation and gas collection. This highlights the fact that most of the PEC device studies do not pay much attention to ion and gas transport in the electrolyte. Nevertheless, they are clearly important for a fully operational, complete PEC system. The area of the lens was 10×10 cm^2, so the active area of the device was also closer to commercial devices than the other examples. The HyCon cell demonstrated a maximum efficiency of 16.8 % [30].

The four prototypes discussed above demonstrate a gradual transition from a tightly integrated PEC device with photoactive electrode to mechanically integrated separate PV and electrolyzer units. These prototype structures differ from each other in the way the light absorption, interfacial electrochemical reactions and mass transport in the electrolyte are arranged geometrical with respect to each other in each device structure. These geometrical differences have important implications to device modeling, as discussed in sections 3 – 6.

2.4. Photoelectrode Architectures

Geometrical considerations are important not only for complete PEC device modeling in the macroscopic scale, but also for the modeling of the electrodes. The majority of the PE structures

studied thus far can be roughly divided into three categories: 1) planar, impermeable electrodes, 2) ordered nano- or microstructures (e.g. arrays of microrods or -wires) and 3) more or less random nano- or microstructures (e.g. randomly stacked nanoparticles). In each case the approach and techniques of mathematical modeling are different due to a different spatial, geometrical arrangements of the electrode material with respect to the electrolyte. The different electrode structures also optimize different aspects of the device operation.

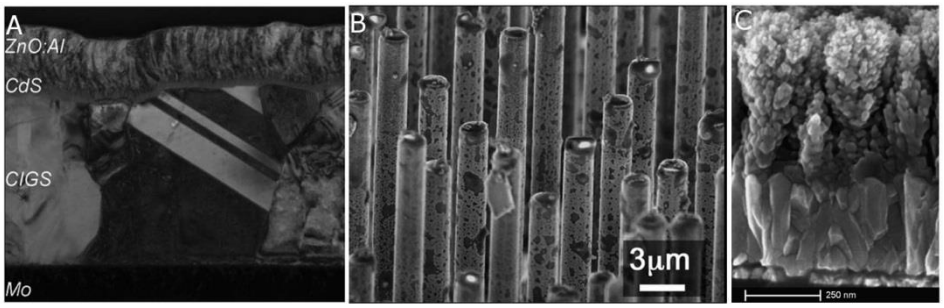

Figure 5. A: TEM cross-section of a CIGS absorber (adapted from Ref. [12] with permission from The Royal Society of Chemistry) B: SEM image of n^+p Si nanowires covered with Ni-Mo catalyst nanoparticles (adapted from Ref. [31] with permission from The Royal Society of Chemistry) C: HR-SEM cross section figure of a mesoporous Si-doped hematite film. (Reprinted with permission from Cesar et al.[32]. Copyright 2009 American Chemical Society.)

2.4.1. Planar Electrodes

From the point of view of the electrode geometry, planar electrodes (Figure 5) are analogous to conventional PV cells, where an electric field separates the electrons from holes. Several devices are based on a buried PV cell, but even in the case of PEC devices many aspects of the operation are similar to PV devices although the field is formed at the semiconductor-electrolyte -interface (SEI), which also determines the relative positions of the energy levels of the PE.

Many high-efficiency device prototypes are based on planar PV cells (e.g. [10–13]). Indeed, the nano- and microstructures discussed below are not required for high efficiencies, but rather, a way to improve the performance of materials that have otherwise comparatively poor charge transport properties. The planar structure may also be an advantage compared with other PE structures, when protective coating methods are considered: A flat surface may allow the use of coating techniques that may not be possible with nanostructures, which could be important for the manufacturing costs and stability of the devices.

Most aspects of the operation of planar PEs/PV cells can be described with a 1D differential equation system[33] that is faster and simpler to solve than two or three dimensional systems. This in turn makes planar electrodes a good model system for fundamental studies [34–36].

2.4.2. Ordered Microwire Array Electrodes

One of the central aims of using nanostructured electrodes is to decouple light absorption and (minority) charge transport from each other. In ordered nano- or microwire array electrodes the minority carriers are transported in the radial direction of the wires, and are therefore almost unaffected by the PE thickness. However, the majority carrier transport occurs along the central axis of the wires and is naturally affected by the length of the wires. Making the rods narrow compared with minority carrier diffusion length helps improving charge collection, but recombination can become a problem with very thin wires, similarly to very small nanoparticles, when the surface/junction area becomes much larger than in a planar electrode[28,32,37].

The wire array devices are currently at proof of concept level. The most recent development was the construction of a device capable of unassisted solar water splitting (Figure 3), but the achieved efficiency was very low[28]. However, the operating principles of the wire array PE or PV such as

charge transport[37], optical properties[38–40], mass transport in the electrolyte inside the array[41] and the general operation characteristics[31,42–46] have been studied for a long time both computationally and experimentally. A recent review[47] summarizes several aspects of Si microwires ranging from manufacturing methods to operation characteristics. Additionally, nanotube arrays made for example of hematite[48,49] and TiO_2[50] have also been studied.

2.4.3. Random Nanostructures and Nanoparticles Electrodes

Other nanostructures can be considered as more or less random, porous material networks. The nanostructured hematite films by Grätzel and co-workers (e.g.[32,51,52]), for example, combine different size scales in their structures ranging from somewhat ordered, almost micrometer-sized features to rough, random nanoparticle surface texture. In these materials the minority and majority carrier transport directions are mostly the same as in the rods and tubes, but the more random structure may create more tortuous paths for the charge carriers. Like in rods, charge transport and light absorption in random nanostructures can be optimized almost independently of each other. Also the size of the structures affects charge collection similarly. Enhancing light absorption with core-shell –nanoparticles, analogous to core-shell wires[39], has also been proposed[53]. An additional effect on charge transport comes from the grain boundaries that induce electron traps that impair charge transport properties[54]. Therefore, in the applications where random nanostructures are typical, rod and tube structures have been considered as an alternative that could enhance charge transport although possibly at the cost of reduced surface area[31,48,55,56].

Having described above the recent trends in the PEC device prototypes and different device and photoelectrode architectures, we turn our focus to the physical processes taking place in them, namely, light absorption, charge transport and electrochemical reactions, and discuss in more detail the different methods used in their modeling.

3. Light Absorption

Light absorption is the starting point of all solar energy conversion processes and therefore fundamental to their theoretical analysis and modeling. The number of photons absorbed in unit time, their energy, and the maximum fraction of the energy that can be converted to useful form determines the ultimate efficiency limits of the process[57,58]. It is somewhat surprising from this perspective that optical modeling of light absorption in PEC devices has received relatively little attention. In many cases when the modeling has not focused on the optical performance of the device, it has been either entirely neglected, e.g. [16,59], or has been included in a simplistic way only to facilitate other calculations[26,60]. Also, the optical properties of water have often been neglected, even though they can affect the device operation noticeably[61]. When detailed optical models have been used their purpose has been to explore possibilities for device optimization specifically by optical design [23,39].

The choice for a suitable optical model depends on the complexity of PE geometry. Both macroscopic and microscopic geometrical features play a role here. Simple ray optics can be used to describe the reflection and refraction of light at macroscopically smooth surfaces and interfaces, but more sophisticated models are needed to account for light scattering and interference effects that arise when the size of the geometrical features is comparable to the light wavelength. The optical models can be furthermore one-, two- or three-dimensional, depending on how many spatial dimensions are needed to describe the electrode geometry and the propagation of light in it. In the following, optical models used in PEC research are surveyed starting from the simplest case.

3.1. Simplified Light Absorption Modeling Based on Beer – Lambert Law

In the simplest case, the photoelectrode can be considered as a homogenous and isotropic planar layer that absorbs light, but does not scatter it, and which is thick enough to make intensity variation due to interference and the wave-nature of light negligible. These approximations are reasonable for example in the case of planar, non-porous semiconductor electrodes [17,18,62]. Another example is nanoparticle based photoelectrodes, where both the particles and the pores in-between them are so small and so uniformly distributed that the effective refractive index does not vary at length scales close to or longer than the light wavelength. In this case, the local light absorption rate in the dimension perpendicular to the electrode surface can be described well with the Beer-Lambert (B-L) law. This simplifies the mathematical modeling considerably and has therefore been used whenever the main focus has been on other things such as the kinetics and charge transport at the photoelectrode, even if the above mentioned assumptions have not been necessarily true [19,60,63–67].

From the mathematical perspective, the B-L law is particularly suitable for solving linear differential equation models of charge carrier generation, transport and reaction, since the exponential form of the light absorption profile allows obtaining analytical solution. Solutions for the steady-state electron (or hole) concentration profile, and the spectral quantum efficiency (incident photon to collected electron –efficiency, IPCE) has been derived this way for situations when the incident light is monochromatic [64,68,69]. One of the most typical applications of these analytical models has been the investigation of the effects of photoelectrode thickness on the photocurrent yield [17,18,60,62].

When the incident light is not monochromatic, but the assumptions of B-L law hold otherwise, the electron-hole pair generation profile is the sum of the exponentially decaying generation profiles of all wavelengths that the material can absorb

$$G(x) = \int_{\lambda_{min}}^{\lambda_{max}} \alpha(\lambda)\phi_0(\lambda)e^{-\alpha(\lambda)x}d\lambda \quad (1)$$

where α (1/m) is the absorption coefficient of the light absorber, ϕ_0 is the incident photon flux (photons·m^{-2}·s^{-1}·nm^{-1}) of wavelength λ, and the integration carried out over the wavelength range where both photon flux and absorption coefficient have nonzero values. Linear differential equation PE models where the generation term is according to Equation (1), or even arbitrary, can be solved with Green's function techniques [70]. Alternatively, Equation (1) can be approximated relatively accurately with a single exponential function, which allows using the readily available analytical solutions directly even when the light is not monochromatic[71].

Although used predominantly for optically thick layers, B-L model applies also to layers that are significantly thinner than the shortest wavelengths in the solar spectrum. For example Trotochaud et al. used B-L model to investigate the compromise between optical and electrochemical performance when the thickness of the catalyst layer covering the PE was varied [19] (Figure 6 in Section 6**Error! Reference source not found.**). The interference effects in catalyst layer were neglected, which made the model simple enough to make calculations with large number of other model parameters feasible. If the catalyst-electrode interface is not an efficient reflector, this simplification will not affect the results significantly, since the considered layers were very thin (less than 20 nm). However, when the system contains a highly reflective interface, interference can be an important factor for light absorption even, when layer thickness is only 10 – 30 nm[23].

Reflection of light becomes important when there is significant change in the refractive index across some important material interfaces, such as at the front air-glass interface of a typical PEC device. Reflection losses due to a single interface can be calculated by the Fresnel equations, taking also into account Snell's law if the angle of incidence is oblique.

3.2. Transfer Matrix Modeling of Multiple Reflections and Interference in Optically Thin Layers

When a planar photoelectrode consists of multiple layers of materials that have a different refractive index, light is partially reflected at each interface, giving rise to forward and backward traveling electromagnetic waves within the layer structure. If the materials do not scatter light significantly, the waves moving in opposite directions are coherent and can interfere with each other producing spatially varying light intensity fluctuations that modify not only the overall reflectance and absorptance of the PE, but also the spatial generation profile $G(x)$. This situation can be treated with optical transfer matrix methods (TMM), that allow solving the Maxwell equations exactly in the stratified 1D layer stack consisting of isotropic and homogenous optical layers taking into account even light polarization (see e.g.[72–74]). TMM is the standard method of choice for designing optical coating and layered structures where interference plays a role.

The effects of interference and light trapping in thin films were illustrated by Dotan et al.[23]. They used a 1D model based on a plane wave solution to Maxwell's equations, to study light absorption in a few tens of nanometers thick Ti-doped hematite films [23]. Their simulations and experiments showed that it is possible to enhance the light absorption and photocurrent generation significantly with a relatively simple, but well-designed PE structure. The photocurrents tripled when ca. 30 nm thick hematite films prepared on Pt reflector instead of a FTO coated glass, since in the former configuration the hematite acted as a quarter wavelength absorber where the local optical field intensity is maximized at the center of the layer. According to the simulations, light absorption could be improved even more with Ag, Al and Au reflectors. However, the experiments were not entirely conclusive on this matter, since the improvements with Ag reflector were achieved with additional modifications to cell structure. Poor charge transport properties were one of the main

reasons why the highest measured and predicted photocurrents were produced with very thin hematite films (20 – 30 nm, depending on the reflector material) [23].

TMM describes stacks of thin layers well, but it runs into problems with thick layers and their interfaces that introduce incoherence into real systems[74]. In addition to resolution limitations and nonparallel surfaces, also scattering at interfaces affects the optical properties of multilayer systems[75]. Additionally, nanostructured materials can scatter light within the layers of the optical stack, so the light absorption profile can differ significantly from the single exponential predicted by B-L law. Light scatterings effects can be simulated for example with numerical Monte Carlo methods, e.g.[76,77], that are applicable not only for planar electrodes but in general. For planar electrodes, approximate modeling of light scattering effects can be carried out analytically with the four-flux model that divides the light flux to forward and backward moving specular and diffuse components [78,79]. It has been used to describe light absorption and scattering in dye solar cells (DSCs)[80] and could be similarly utilized with nanostructured PEs of PEC devices. Another popular approach is the scalar scattering theory although rigorous solvers for Maxwell's equations are used increasingly often as computational capacity increases[75].

3.3. Solving Maxwell's Equations in Complex Electrode Geometries

When it comes to more exotic electrode geometries such as wire arrays and rod structures [37,42], more sophisticated optical models are needed. Although wire arrays appear planar at the macroscopic scale, their internal structures cause optical effects that cannot always be described with the 1D models[45]. Typical problems with wire arrays are that a significant fraction of the electrode volume does not absorb light and the rods create a relatively regular pattern that causes problems with diffraction, as Kelzenberg et al. demonstrated experimentally in their study about the optical properties of Si microwire arrays [38]. One example of the methods used in 2D and 3D

geometries are finite difference methods that have been used in simulating the optical properties of different nanowire structures[40,46].

Detailed optical modeling of wire array electrodes is possible by solving the Maxwell's equations in the simulated geometry, which allows accounting for scattering, absorption and diffraction. This was demonstrated for a single wire by Mann and Garnett who modeled the optical properties of Si nanowires with and without a Ag core and showed that the Ag core enhances light absorption [39]. Because they performed the simulations by solving the Maxwell's equations, they were able to separate the polarization components of light and show that the most significant absorption enhancement was due to the polarization-dependent resonances becoming almost polarization-independent, which improved the absorption of the transverse electric component (no electric field in the propagation direction). The core-shell structure enhanced the absorption coefficient in particular at the long wavelengths of light due to lower radiative losses of high order resonance modes[39]. The core-shell scheme could therefore be interesting for boosting the performance of both PV and PEC devices at the longer wavelengths where the light absorption is usually the weakest. A similar core-shell approach to spherical TiO_2 (core)/hematite (shell) nanoparticles has also been studied with optical simulations[53]. An important effect discovered with the particles is that placing them near each other, i.e. constructing an electrode, deteriorates their light absorption properties significantly[53].

Overall, the optical behavior of the PEC devices depends both on the material properties (optical constants) and the device and electrode geometry. The examples discussed above demonstrate how these geometrical designers can be guided by optical modeling. The optical models can describe how electrode geometries influence the optical performance even in the presence of complex optical phenomena such as interference, scattering and diffraction, and relatively arbitrary choices

of materials. On the other hand, the optical constants required as an input to these models are more difficult to derive purely from the theory, but can be attempted with first principles methods although at high computational costs [81,82]. Recent advances in computational methods have allowed calculating the absorption spectra of for example tungsten trioxide (WO_3)[83] and silicon (Si)[82] from the first principles even though these materials have indirect bandgap, which complicates the calculations compared with direct bandgap materials, because the light absorption process in them involves phonons in addition to photons and electrons. As the computational resources increase and the methods advance, we could expect to see first principles methods play an increasingly important role in the optical design of PEC materials in the future.

4. Charge Transport and Recombination

The goal of all water-splitting PEC devices is to drive hydrogen and oxygen evolving interfacial electrochemical reactions by the free energy stored either in the photogenerated electrons in the CB or holes in the VB. For these reactions to occur, the charge carriers have to move to the interface from their point of generation, which is called charge *transport*. All other reactions that lead to an electron being removed from CB and hole from the VB are called *recombination* reactions. For a given carrier generation rate, the interfacial reaction rate thus depends on how fast charge transport is compared with the recombination. As a result of this competition, only a fraction of charge carriers reach the surface before recombining. This fraction is called charge carrier *collection efficiency*.

The theoretical basis for the abovementioned processes comes from well-known semiconductor device physics described well in several textbooks [84,85]. In general, the charge transport is driven by diffusion in a concentration gradient and drift in an electric field [84–87]. Together with carrier

generation, recombination, and interfacial reactions, this leads to carrier concentration distributions that can be determined by solving the device physics equations with appropriate boundary conditions. These basic equations, which are summarized briefly below, will serve as a reference point for the discussion about charge transport and recombination modeling in the subsequent sections.

4.1. Drift-Diffusion Model

The centerpiece of the physical modeling of PEC photoelectrode is the charge carrier continuation equation

$$\frac{\partial c_i}{\partial t} = \nabla \cdot \vec{J_i} + G - R_i \tag{2}$$

This partial different equation essentially says that the time evolution of the charge carrier (i = electron, hole) concentration (c_i) in a unit volume element is caused by the net flux ($\vec{J_i}$) of the carriers into it, and their generation (G) and recombination rate (R_i) in it.

The optical generation rate of electron-hole pairs given by Equation 1 has already been discussed in the previous section. Here it is important only to note that Equation 2 is indifferent to the actual optical model used: any optical model can be used to give the generation term G. This means that as far as the electrical and electrochemical operation of the photoelectrode does not change its optical properties (e.g. via electrocromic effects), optical modeling can be carried out separately from the electrical modeling, which applies not only to Equation 2, but in general.

As already mentioned, charge transport is driven by concentration gradients (diffusion) and electric fields (drift). The total flux of species i according to drift-diffusion model is

$$\vec{J_i} = -D_i \nabla c_i + z_i c_i \mu_i \vec{E} \tag{3}$$

where μ_i is the mobility of the species, z_i its charge and $\vec{E}$ the electric field. The mobility and diffusion coefficient are connected to each other by the Einstein relation

$$D = \frac{\mu\, k_B T}{q_e} \tag{4}$$

where q_e is the elementary charge, k_B the Boltzmann constant and T the absolute temperature. This allows simplifying the flux as

$$\vec{J_i} = -D_i\left(\nabla c_i - \frac{z_i c_i q_e}{k_B T}\vec{E}\right) = -\mu_i\left(\frac{k_B T}{q_e}\nabla c_i - z_i c_i \vec{E}\right) \tag{5}$$

The operation of most PEC devices is based on the separation and transport of charge carriers in an electric field (2nd term Equation 5) close to the SEI, whereas diffusion (1st term Equation 5) may be the dominant transport mode in the bulk of the semiconductor where electric field tends to zero. The distribution of the electric field at the SEI can be described by the concept of *band bending* (BB). According to electrostatics, electric field is associated with a gradient in the electrostatic potential ϕ, which in the energy band diagrams can be visualized as gradient (bending) of the band edges (see Figure 3), expressed mathematically as $\vec{E} = -\nabla \mathrm{V_{BB}}$. Band bending is thus a convenient graphical tool for representing the spatial variation of electric potential near semiconductor junctions and interfaces, and has become a central concept in the description of the physics of PEC photoelectrodes. We can see its effect on the continuation equation (Equation 2), by inserting the expression for the flux (Equation 5), expressing the electric field in terms of band bending, and making the typical assumption that the diffusion coefficient is a constant and isotropic

$$\frac{\partial c_i}{\partial t} = -D_i\left(\nabla^2 c_i + \frac{z_i q_e}{k_B T}\nabla \cdot (c_i \nabla \mathrm{V_{BB}})\right) + G - R_i \tag{6}$$

Several different mechanisms can cause band bending. For example, a recent review discusses the physical phenomenon and its effects on photocatalysis [87] and another recent article provides a method for the accurate calculation of band bending in doped semiconductors [88]. In most cases, however, only a few main features may need to be included to describe the operation of a typical PEC photoelectrode. According to the simple depletion region model, the band bending is caused by net charge density in the depletion zone of the semiconductor

$$\nabla^2 V_{BB} = \frac{-\rho}{\varepsilon_{sc}\varepsilon_0} \tag{7}$$

where ε_{SC} is the relative dielectric constant of the semiconductor and ε_0 that of vacuum. The net charge density, ρ, comes from the local density of ionized donor (N_D^+, N-type semiconductor) or acceptor (N_A^-, P-type) atoms and the CB electrons and VB holes (If trap states were present, their charge would be included too)

$$\rho = q_e(N_D^+ - N_A^- - n + p) \tag{8}$$

Typically almost all dopant atoms are ionized, meaning $N_D^+ \approx N_D$ and $N_A^- \approx N_A$. Other common approximations are that both electron and hole densities are small compared with dopant ion density, that there are only either donors or acceptors in the material, and that the material outside the depletion zone is charge neutral. These assumptions together with Poisson's equation of electrostatics give a depletion zone width that depends on the square root of the potential difference over the depletion zone. For an N-type material, the width of the depletion zone is

$$w_{depl} = \sqrt{-2\frac{\varepsilon_{SC}\varepsilon_0}{\rho}\Delta V_{depl}} \approx \sqrt{-2\frac{\varepsilon_{SC}\varepsilon_0}{q_e N_D}\Delta V_{depl}} \tag{9}$$

A negative value of ΔV_{depl} corresponds to "upward" band bending, positive for "downward" in the electron energy diagram, i.e. opposite to the sign of the charge density ρ in the depletion zone. Also the geometry of the depletion zone affects the situation. Eq. (9) applies to the situation in Cartesian coordinates in one dimension. In polar (e.g. the radial direction of a cylindrical nanorod) and spherical coordinates (e.g. nanoparticles) the relation between depletion width and potential difference may be more complicated, depending on the boundary conditions.

Finally, we point out that the effects of concentration and band bending can be combined (and generalized) to a single term, the *electrochemical potential* of the charge carriers (electrons or holes), whose gradient gives the flux of the carriers in question[63,85–87]. The electrochemical potential takes into account also differences in the bulk conduction (CB) and valence band (VB) levels across semiconductor junctions [85].

Having summarized the basic theory of the drift-diffusion model, we now go one step further behind the above equations to discuss how theoretical modeling has been used to explain the underlying physical phenomena. In the same way as with the optical modeling, we make the distinction between effects arising from the electrode geometry and to the effects related to the material properties.

4.2. Electrode Geometry and Size Effects

As with optical modeling, charge transport in planar, compact electrodes can be described well with a 1D model, whereas in the case of more complex electrode structures such as the semiconductor wire and rod arrays, as well as with nanoparticle based electrodes, geometrical and size effects come into play. Since the reaction rate of the water splitting interfacial electron transfer reactions is determined by the electron and hole concentrations at SEI, in addition to the reaction

kinetics discussed in section 5, it is essential for accurate PEC photoelectrode modeling to get these surface concentrations right. Here, size effects related to band bending and the transport lengths of electrons and holes become important and require 2D or 3D models.

If the nanoparticles are randomly packed, the PE film may be considered as a macrohomogenous effective medium when it comes to the charge transport. If the film is macroscopically planar, this reduces the mathematical description to one dimension, which simplifies the mathematical modeling significantly. These 1D models, e.g. [60,63,71,89], have much in common with, or are directly based on, the original model of Södergren et al. for DSCs[64]. The simplicity of these models however comes with the cost that they are described with macroscopic "effective" parameters, the values of which more or less depend on the specific microscopic structure of the electrode under investigation. For this reason, these models are most useful for top-down interpretation of experimental data in terms of the effective transport and recombination characteristics, but when it comes to bottom-up modeling, more detailed transport models are needed to predict the values of these macroscopic parameters.

This said, it could still be possible to account for the microscopic geometric effects in a macroscopic effective medium model, if the parameters of the 1D model were quantitatively linked to the microscopic properties through physical models. For example, the slow transport of holes to OER catalyst could be represented with a lower reaction rate constant, thereby embedding the detailed information on the microscopic processes in the representative numerical value of a single rate constant. This approach would turn rate constants into voltage-dependent functions, similarly to phenomenological rate constants used in analysis of intensity modulated photocurrent measurements[90–92].

Whenever the distance to the nearest electrolyte interface everywhere within a semiconductor particle or layer is much shorter than the full width of the depletion zone that would develop if there was enough room for it (see Equation 9), the particle or layer can be considered fully depleted from (or accumulated by) charge carriers without much curvature of the bands and therefore electric field within it. This leads to a model, where transport is mainly driven by diffusion. At first, it would seem that even in electrodes the size of the structures would most likely affect charge collection very similarly to the size of the individual photocatalyst nanoparticles with diffusive charge transport [65,93,94]: When the diffusion length is large compared with the structure size, bulk recombination can be neglected and the quantum yield is affected only by surface recombination [93]. In contrast, when the diffusion length is very short compared with the size of the structures, charges created in the bulk will recombine before reaching the interface[93], and hence transport can be neglected, because those charges that manage to get to the surface appear as if they were stationary since they did not come far from it. In the intermediate cases, the quantum yield depends strongly on the ratio of the nanostructure size and diffusion length, and neglecting this interplay could lead to significant errors[93].

The operation of wire structures has been analyzed in detail with 2D simulations that included also the electric fields[44,95,96]. There are some similarities, but also striking differences, to individual nanoparticles. The results indicate that high quantum yields (short circuit current) can be achieved even with short carrier diffusion lengths by reducing the wire radius, but too short a radius actually results in very low quantum yield[95,96]. This is contrary to the nanoparticles that show monotonic increase when particle size decreases[94]. The yield is reduced when the wire radius becomes so small that the inversion layer (where minority carrier concentration is higher than majority carrier concentration) near the surface occupies a significant fraction of the total electrode volume, so that

recombination near the surface dominates device operation[95,96]. This situation corresponds to operation in high-level injection conditions, meaning that electron excitation rate (i.e. light intensity) is sufficiently high that the concentrations of electrons and holes are higher than the dopant density and approximately equal to each other, which increases the recombination rate in the device[95,96]. This in turn is typically considered to reduce both current density and voltage significantly although it might be possible to achieve high currents and voltages with discrete selective contacts, analogously to point-contact solar cells[44,96]. Because the high injection criterion depends also on the dopant density, increasing it allows high charge collection efficiencies, if a sufficient increase is possible within material constraints[44,96]. Near the substrate contact the collection efficiency remains high, because the majority carriers do not need to travel a long distance, so they can be collected before recombining[95]. This situation with a short collection path for both minority and majority carriers is similar to individual nanoparticles, but farther from the contact the longer collection path of majority carriers makes the collection efficiency more sensitive to charge transport and recombination[95]. Also, open circuit voltage is significantly affected by the recombination kinetics, so considering only short circuit current or diffusion length is not sufficient for understanding the operation of the devices, especially when the voltage may behave counter-intuitively, because charge transport properties affect it in a different way than in planar devices[96]. Therefore, too simplified models based on planar devices may not necessarily describe nanostructures well.

4.3. Material Properties

Geometry is not the only challenge that nanostructured materials present to charge transport modeling. Nanocrystalline materials have typically plenty of structural imperfections at smaller length scales than what can be described by the modeling geometry, such as grain boundaries and

dislocations that may dictate their macroscopic properties. Obviously, the whole electrode surface itself is an imperfection of the crystal structure and gives a variety of trap states associated either to the crystal itself or the surface adsorbed electrolyte species. Predicting macroscopic transport and recombination properties purely form the theoretical stand-point is therefore challenging. To give an example of these modeling challenges, we discuss in the following how it has been attempted in the case of colloidal metal oxide semiconductor photoelectrodes.

4.3.1. Transport Properties

Nanostructured, colloidal materials often exhibit anomalous charge transport. The charge transport can be for example very slow compared with crystalline semiconductors and the diffusion coefficients can depend on the electron density and the particle size [54,97–99]. The anomalous transport is thought to arise from the disorder of the material that creates localized electron states that act as traps and affect the macroscopic transport and recombination properties [54,100]. In many cases, the trends of diffusion the coefficient and electron lifetime appear to be conveniently opposite, making the diffusion length of electrons roughly constant[54]. Therefore the traps do not necessarily pose a significant problem for modeling, if only rough estimate of steady state diffusion length is of interest, but has to be taken into account when modeling transient behavior[100].

The exact origin and location of the traps is still debated and several different theories have been proposed[101]. Based on how photocurrent, charge density and diffusion coefficient behave with respect to each other and the size of the nanoparticles, it appears that the traps are mostly located at the surface of the nanoparticles, at least in TiO_2[102]. Additionally, recent first principles calculations and photoluminescence measurements indicate that the electron traps in TiO_2 are caused by under-coordinated Ti atoms at the edges of the particles that create localized low-energy surface states[101,103].

The trapping/detrapping behavior of electrons (in metal oxides) is often modeled with either multiple trapping (MT) or Miller-Abrahams hopping (M-A) model[54]. They are often considered as alternatives to each other, even though MT model is more of a special case of the hopping model[54]. Based on simulation results, the M-A model appears to describe experimental results more accurately than the MT model[97,100], but both models have been used to study the effects of trap states on electron transport with random walk numerical simulations[100,104,105].

Random walk simulations of nanoparticle electrodes with varying degrees of disorder carried out by Anta et al. have shown that reducing the randomness of the electrode morphology improves charge collection significantly, but only when the charge transport properties of the disordered materials are "intermediate"[54,104]. If the charge transport is efficient to begin with, there is almost no room for improvements, and when the charge transport properties are poor, the improvements in the electrode structure are not enough to compensate for the shortcomings in the material properties[54,104]. However, with intermediate properties, the modeling gave up to a factor of two improvements in the collection efficiency (from $\eta \approx 15$ % to $\eta \approx 30$ %) in the case of somewhat ordered electrode structure that forces the electrons to a more direct path across the electrode while restricting their lateral movement in the plane of the electrode, i.e. when the movement of electrons is more confined to one dimension[104]. It is unlikely that modifications to electrode geometry alone would be sufficient for good efficiencies, meaning that material properties also need to be improved sometimes. An example of a method that apparently accomplished improvements in both geometry and material properties is the anodization method that Mohapatra et al. used to manufacture hematite nanotube arrays [48]. Because the nanotubes did not have boundaries similar to those between nanoparticles, charge transport resistance was decreased by a factor of 40 – 50

and current density was almost sixfold compared with the best results obtained with the other studied nanostructures.

The structure of bulk material determines the spatial distribution of energy levels in the material and this in turn gives the charge transport mechanism and its kinetics. When the electronic wavefunction of the material is sufficiently delocalized, the motion of charges can be described as the motion of nearly free charges (i.e. with the effective masses)[106], and the electron and hole mobility can be determined from the calculated energy band structure of the material. Examples of the such energy band calculations can be found in the literature, either with[107] or without[82,108,109] calculations of the mobility or effective mass of charge carriers.

However, there are also materials, where the electron wavefunction is strongly localized due to electron-electron interactions (Mott insulators), and in their case charge transport is described with hopping behavior[106]. In many metal oxides, for example, polaron hopping is considered to be the most significant charge transport mechanism[106] and the related energetics have been studied with first principles simulations at least for α-Cr_2O_3 (chromia), TiO_2 (both anatase and rutile) and α-Fe_2O_3 (hematite)[110–114]. In addition to electron transport in pure materials, both hole transport and the effect of dopants have been studied for hematite, and simulations indicate that some dopants may create new charge transport channels in addition to the polaron hopping of the intrinsic material[112,114]. These studies also underline some of the problems with DFT calculations: In the case of both TiO_2 and hematite the simulations suggest that electron mobility in one kind of material (rutile, Ti-doped hematite) would be higher than in another type of material (anatase, Si-doped hematite) whereas the opposite is found experimentally [111,114]. In both cases several factors that may affect the properties of real materials, could not be simulated [111,114]. Somewhat similarly, compared with other dopants, doping hematite with manganese (Mn) did not improve the

conductivity of the intrinsic charge transport channel, but since Mn can exist in hematite in both +2 and +3 states, it may, according to the simulations, create a new high mobility hole transport path through Mn atoms[112]. Because Mn can be doped into hematite at very high concentrations, it may be possible to extend the local effect throughout the material, which could in part explain the conductivity improvements achieved with very high concentrations of Mn[112,115].

Overall, charge mobility can be anisotropic in the microscopic scale [112,114], depending on the atomic structure of the material in question, but in the macroscopic scale isotropic diffusion coefficient (or mobility) is often used, because the different orientations of the crystallites typically average each other out. On the other hand, the performance of the PE can be improved at least to some extent, if the crystallites can be aligned preferentially for charge transport so that the effect of grain boundaries is reduced[52].

4.3.2. Recombination Kinetics

Recombination can proceed through several mechanisms, but typically one or two of them are more significant than the others, depending on the system in question. Correspondingly, the mathematical form of the expression for the recombination rate R_i in Eq. 2 can be different for different recombination mechanisms, but is always a function of the reactant concentrations (electrons, holes, electrolyte species) and the rate constant of the reaction. Including recombination in the transport models involves finding the correct rate expression and determining or calculating the values for its kinetic constants.

All recombination mechanisms taking place in the bulk of the semiconductor depend on both electron and hole concentrations, but in some simple cases it is possible to make approximations that enable expressing the recombination rate as a function of only the minority carrier

concentration[84]. However, there can also be surface recombination mechanisms that involve only electrons or holes. For example, in the regenerative electrochemical solar cells, where majority carriers can react with the oxidized or reduced component of the redox couple (depending on whether the semiconductor is n- or p-type) this recombination mechanism does not depend on the minority carrier concentration, but only on the concentration of the majority carriers and the redox couple[64,68]. Although water splitting cells are not regenerative solar cells, recombination of majority carriers may still occur with surface adsorbed intermediates of the OER and HER that are both complex multi-step, multi-electron transfer processes. The rate expression would be in this case similar to Shockley-Read-Hall (SRH) or surface state recombination, as it would depend on both the majority carrier and surface adsorbate concentration[60,66].

The recombination rate constants are typically determined experimentally and there is a large variety of experimental techniques for this purpose. On the contrary, to the best of our knowledge, there are no computational studies that would have tried to calculate either the surface or bulk recombination rate constants of PEC materials from the first principles. First principles calculations of recombination kinetics have been more common in other fields such as optoelectronic devices, like light emitting diodes (LEDs) and have been presented for Auger recombination for example in GaAs[116] and different nitrides[117], and also for SRH recombination in InAs[118]. These studies may provide a starting point for similar calculations for PEC materials, but one has to keep in mind that different operating conditions of the devices may need to be taken into account in the calculations (e.g. different dopant densities or injection conditions).

5. Interfacial Reactions

Both HER and OER are multi-electron transfer reactions that proceed via intermediate single electron transfer reactions involving their intermediate reaction products. The reaction processes and kinetics depend only on the conditions at the interface (reactant concentrations, potential and energy levels) and therefore the electrode structure affects the reactions only via the surface facets of the interface, differences in mass transport and the resulting concentration differences at the interface. The planar, compact electrodes are preferred in characterization studies, because the conditions at the interface are more uniform than in nanostructures, where mass transport causes differences inside the structure. One should nevertheless keep in mind that since the interface area is significantly smaller than in a nanostructured electrode, the current density at the interface is higher at any given total current, which leads to higher kinetic overpotentials, unless a lower total current is used in the experiments. The interpretation of the results and their application to modeling nanostructured electrodes thus need to consider the effects of reaction surface area carefully. Both nanowires and random nanostructures are similar in a sense that the electrolyte interface extends throughout the electrode, and concentrations are affected by mass transport in the electrolyte. In the case of wire structures a more direct path may allow faster transport, and random nanostructures may have more interfacial area, but otherwise the interface kinetics are similar, if the conditions are the same.

5.1. Kinetic Models of Interfacial Electron Transfer

The most common ways to model electrochemical reactions on metal electrodes Butler-Volmer (BV) and Tafel equations. Although BV equation is based on single-electron transfer reactions, it can be generalized for multi-electron transfer reactions as well, because one of the intermediate one-electron reactions is the rate limiting step (RLS) of the total reaction, and therefore determines

the current-overpotential behavior of the total reaction in steady state[119]. For example, the BV equation for a multistep reaction $Ox + ne^- \rightleftarrows Red$ that consists of single-electron transfer steps is[119]

$$i = i_0 \left[\frac{C_{Ox}}{C_{Ox,0}} \exp\left(\frac{-(n_b+\alpha) q_e \eta}{k_B T} \right) - \frac{C_{Red}}{C_{Red,0}} \exp\left(\frac{(n_a+1-\alpha) q_e \eta}{k_B T} \right) \right] \quad (10)$$

The transfer coefficient of the RLS is α and for the reduction of *Ox* the number of transferred electrons before the RLS is n_b and after RLS n_a (and so $n_b+n_a+1=n$). The exchange current density of the total reaction is i_0 and it depends on both the exchange current of the RLS and the RLS itself (n_b, n_a and α)[119]. These dependencies on the RLS enable analyzing the reaction mechanisms from experimental data in terms of the exchange current density and RLS[119]. The elementary charge is denoted with q_e, Boltzmann constant with k_B, the temperature (in Kelvins) with T and the overpotential is η. Concentrations of the reduced and oxidized species of the total reaction are C_{Red} and C_{Ox}, and 0 in the subscript denotes their equilibrium concentrations ($\eta = 0$).

When modeling electrochemical reactions in a device, the exploration of different possible reaction mechanisms is typically not important, so the following/preceding number of electrons (n_a or n_b) and α can be written as a single anodic or cathodic transfer coefficient, whose value is based on experimental data[21,59]. Also, when the stoichiometric coefficients of the reactants and/or products differ from one, the concentration fractions (activities) need to be raised to the power of their stoichiometric coefficients to preserve the correct concentration dependence of the Nernst potential (η when $i = 0$)[21,59].

At low overpotentials HER on Pt can be described accurately with BV equation in both alkaline and acidic conditions[120,121]. However, until recently there has been uncertainty about the reaction mechanism (and thus the charge transfer coefficient) and kinetics on noble metals, despite HER

on Pt being one of the most studied reactions in electrochemistry[122]. Also, possible differences between hydrogen adsorbed on the surface at different potentials have been studied[120,123,124] and the possibility of the reaction proceeding simultaneously through two different pathways has been considered[124,125]. Most recent results strongly indicate that many of previous results are due to mass transport masking the reaction kinetics, and therefore it needs to be considered carefully especially in characterization studies [120,123,126–128]. OER is an even more complicated reaction sequence than HER, but BV has been used to model it as well[21,59].

In contrast to metallic electrodes, the reaction rates at the semiconductor surface depend on the concentration of electrons or holes (depending on the reaction/type of the semiconductor) at the interface [89,129–131]. The current density of the charge transfer reactions are typically expressed simply as [18]

$$i = q_e k^{red}(n_0 - n) \qquad \text{P-type semiconductor} \qquad (11a)$$

$$i = q_e k^{ox}(p - p_0) \qquad \text{N-type semiconductor} \qquad (11b)$$

Where n marks electron and p hole surface concentration. In both cases subscript 0 denotes the equilibrium concentration of the species in question that depends on the potential levels at the interface (i.e. CB/VB level and reaction potential)[18]. The effective rate constants k^{red} and k^{ox} depend not only on the reaction kinetics, but also on the surface concentration of the electrolyte species taking part in the reaction, in a way that depends on the details of the reaction mechanism. The forward reaction rate is controlled by the electron/hole concentration that is affected by the external applied potential, but the potential difference across the interface, and thus the equilibrium concentration, is fixed (in an ideal situation)[18]. When it is taken into account that the concentrations of electrons and holes depend (to a good approximation) exponentially on their quasi-fermi level,

this expression is equivalent to the diode equation although it is not explicitly visible in the presented form[85]. However, if the electrodes are covered with a catalyst, its properties affect the reaction kinetics and also the catalyst-semiconductor interface[20,132]. In practice this means that the effects of the catalyst cannot necessarily be described only as an enhancement of the rate constant or a BV equation that replaces equation (11), but the physical behavior of both interfaces and the catalyst itself have to be considered carefully[20,132].

More accurate description of the reaction kinetics will require modeling each reaction step and the interactions between the intermediate products and reactants. With sufficient knowledge about rate constants and intermediate species this should be possible, and there are already models that can describe the kinetics of multi-step reaction sequences, such as OER[60,65,66,93,94]. Some of these studies have also included a charge transport model to include the effect of electron and hole transport on their surface concentrations and thus on the reaction rates[60,93,94].

Despite offering a very detailed and robust method of describing the reactions, the models containing all intermediate concentrations may not see much use, except in very specific studies. Their problem is that while the theoretical description of the reaction sequence requires several rate constants[125], a single rate constant may be enough to fit the experimental data[127]. This means that the rate constants of other than the rate limiting step (RLS) may not be available experimentally, so there might not even be enough information available for realistic simulations with the multistep models. This is not a problem from the practical point of view of performance optimization as long as the experiments allow identifying the RLS, because improving the other steps would not improve the overall reaction rate as effectively as improving the RLS.

5.2. First Principles Studies of Photoelectrochemical Reaction Mechanisms

The first principles methods are derived from quantum mechanics and generally can be divided into many-electron-wavefunction –based and density functional methods (density functional theory, DFT)[15,133]. DFT-methods have become almost a standard way of performing electron structure calculations on surfaces, clusters and solids, among others[133]. The advantage of first principles methods is that they give access to detailed information about the origin of different physical phenomena and experimental observations that could be very difficult or impossible to access empirically[134]. They can also be used to calculate material properties relevant to charge transport[110–114] and optical properties[82,83,135], as was briefly discussed in the previous sections. In this section, we discuss in more detail how first principles methods have been applied to the study of interfacial reaction mechanisms relevant to PECs.

Finding efficient catalysts for both HER and OER is crucial for reducing the losses of the water splitting devices. In this process first principles methods, such as DFT calculations, are invaluable tools for modeling the thermodynamic and kinetic properties of the reactions in different interfaces[15,133,134,136–139]. This information can be useful in designing new catalyst materials by reducing the amount of trial and error in the total process[140]. One problem with both reactions, especially OER, is that they are multi electron transfer reactions that proceed through single electron transfer steps, which complicates the design of catalysts for these reactions[137]. In the case of OER, the catalyst design is further complicated by the fact that the exact reaction mechanism is not known although different schemes have been suggested and studied[141–144].

5.2.1. Thermodynamic and Kinetic Aspects of Multistep Electron Transfer Reactions

For a reaction where one or two electrons are transferred, it is in principle always possible to choose or design a catalyst that is thermodynamically optimal, meaning that at the formal thermodynamic potential of the total reaction, the Gibbs free energy change is zero for all reaction

steps[137]. In other words, barring activation barriers, the reaction is thermodynamically reversible. The problems of the catalyst design increase, when there are more than two intermediate reactions and when the equilibrium potentials of the intermediates are not independent of each other, which can occur if all intermediates interact with the surface through the same atom configuration[137,138,145]. In such a case it is possible that no catalyst will be thermodynamically optimal. In this case significant overpotential would be required to drive the reaction, because the rate constants depend exponentially on the free energy differences[137,141,145]. Unfortunately, the OER is a prime example of such kinetically impaired multi-electron transfer reaction for several known catalysts[137], and is therefore the main performance loss factor of solar water splitting devices. These problems are well illustrated by the first principles calculations about OER on metal and metal oxide surfaces. According to the calculations, the free energies of the reaction intermediates scale in a way that makes all metal and metal oxide surfaces thermodynamically suboptimal for OER[137,138]. However, it may be possible to design thermodynamically optimal catalysts even for multi-step reactions (or at least go beyond the limitations of bulk materials) by using surfaces, whose interactions with the adsorbed molecules are not described by only one parameter[146,147].

A typical simplification made in the reaction energy calculations is to neglect activation barriers and calculate only the energies of the reaction intermediates. Without the activation barriers the free energies of the intermediates show the main trends of what reactions limit the overall reaction rate, how high overpotentials are needed to overcome these limitations, and the main trends of the reaction kinetics[137]. Taking the barriers into account does not change these properties, but yields a more detailed description of the energy levels associated with the studied reaction sequence[137,141].

Therefore the results also contain likely more information about reaction kinetics, which might be useful in the detailed studies of reaction mechanisms and catalyst properties.

5.2.2. Practical Limitations of Density Functional Theory Calculations

The number of atoms that can be included in the system calculated with first principles methods is limited in practice by the available computational power and time. For this reasons DFT studies typically focus on well-defined surface constructions that serve as a model of the real surfaces that can be expected to have a more heterogeneous structure[14]. For example, when nanoparticles are studied computationally, the calculations may need to be restricted to their most active sites [148]. Nanoparticles that are small enough to be calculated as a whole are an exception to this[149].

Real surfaces and particles are a mixture of different crystal facets and may therefore exhibit overall properties that do not correspond to any single facet. This can be managed by calculating each surface separately, and estimating their contributions based on their fraction of the whole surface area, assuming that the properties of the different surface facets are independent of each other[140,148]. This assumption is good in metallic particles, where the freely moving electrons can screen electronic interactions between the different surface facets [140,150,151]. However, when the size of the catalyst particles becomes smaller than the screening distance, the different surfaces may no longer be independent [140].

It is also possible that different surface facets of the same material yield different products from the same reactants, or at least that the fractions of the reaction products differ from one facet to another[152,153]. This can potentially complicate the design of catalysts that should be highly selective for one product. A catalyst may also be selective for a wrong reaction product, which appears to

be the case, for example, with all known candidates for the production of ethanol from synthesis gas [154].

The first principles calculations of photocatalytic reactions become particularly problematic if the surface configuration of the catalyst depends on the operating conditions. Results of Trainor et al.[155] had indicated that, in contact with liquid water, hydroxide-terminated hematite surfaces are the most stable ones. However, later both Hellman and Pala[156] and Nguyen et al.[157] showed that the most stable surfaces turn out to be those terminated by oxygen, when the illumination, which determines the quasi-fermi level of holes, is also taken into account in the calculations.

Also the calculation methods themselves need to be chosen carefully to avoid methodical bias in the results. Self-interaction errors of pure DFT are one example of such difficulties, for which different interaction formalisms have been suggested as a correction[15,133]. These methods, usually called DFT+U, treat the strongly correlated Coulombic and exchange interactions within atoms similarly to Hartree-Fock theory[15]. However, these corrections can create problems of their own, because they generally depend on additional parameters that are obtained either from other first-principles methods (e.g. Hartree-Fock calculations) or experimental results [15,158]. It can be possible that the corrections that best describe bulk and surface properties are different, as one value is typically not optimal for all properties[156,159,160]. In that case not taking the difference into account could affect simulation results, as demonstrated by recent studies about OER on hematite surface[156–158]. Pure DFT has been considered to describe the surface properties of hematite better than DFT+U although this may not actually be the case[156,159,160]. Nevertheless, it has been used to study OER on hematite surfaces, and compared with DFT+U the simulations yielded significantly different free energy changes for the reaction steps, and even a different RLS for the same surface on one occasion[156–158]. The possibility for different correction parameter values for bulk and

surface may be significant for PEC devices, because both the bulk properties, such as the CB and VB energies, charge mobility and light absorption, and the surface properties, such as reaction thermodynamics and kinetics, and stability in contact with the electrolyte, are equally important.

Another significant limitation of DFT is the difficulty related to analyzing reaction steps that are not electrochemical by nature. This difficulty is associated to the commonly used method to include electrochemical reference potential (standard hydrogen electrode, SHE) in the simulations via electrons and protons[14,15]. This can limit the ability to estimate even (seemingly) simple reactions, such as HER/HOR that, at least on some surfaces, proceed through the Tafel step[127,128], where two hydrogen atoms combine into an H_2 molecule, or the molecule breaks into two atoms, without electron transfer to/from the electrode. We note that DFT has been used for calculations about non-electrochemical heterogeneous catalysis, such as ammonia synthesis[148,161], so this is most likely a limitation related to electrochemistry and reference potentials.

Finally, it should be noted that basic DFT is a steady-state method and therefore can be used to calculate only the ground state of the system, whereas the description of excited states requires simulations with time-dependent DFT (TD-DFT)[15,133]. For example, DFT can be used to compare the ground-state energies of different atom configurations or charges in different locations in a crystal lattice, but it does not tell how transitions between these states or locations occur. In TD-DFT, on the contrary, also the energy of the intermediate, non-equilibrium configurations through which the system evolves during the transitions from the initial to the final state are calculated, and based on the obtained energy landscape, the energetically most favorable path can be concluded [15,133,162]. This method, however, is costly computationally since many trajectories with slightly different initial states need to be calculated to collect enough statistics to accurately determine the reaction pathway[162]. This is reflected for example in the computational study by

Akimov et al.[162], who calculated only the RLS of OER on GaN surface, instead of computing the whole reaction sequence. Furthermore, to provide computational efficiency necessary for the time-dependent calculations, they did the calculations with pure DFT instead of DFT variants with electron self-interaction corrections[162].

5.3. Reactant Concentration and Mass Transport in Electrolyte

Mass transport in the electrolyte to and from the catalyst surface affects the steady state surface concentration of the reaction species and thus the reaction rate (current density). Details of the mass transport processes at the catalyst surface have so far received very little attention. This is perhaps because the development of the PE/PV components has not yet reached a state where current densities would have been high enough to be limited by mass transport. Nevertheless, recent studies clearly show that mass transport in the electrolyte can cause significant problems, unless the device is designed properly [16,41,59,163].

For example, diffusion in nanostructured electrodes may prove problematic, when the electrode thickness is increased, if the current density is high enough to cause the depletion of the reactants deep in the film [41]. Another situation where mass transport issues appear is when the electrolyte flowing past the electrodes becomes saturated with O_2 and H_2 forming gas bubbles, which could lead to reduced illumination intensity at the electrode surface[16]. Saturation can be avoided by increasing the electrolyte flow rate, which in poorly designed reactor geometry might also lead to vortices in the electrolyte flow, and consequently the reactants could not be supplied to and the products could not be removed from some parts of the electrodes[16].

In a complete PEC device, mass transport takes place not only in the vicinity of the electrodes but also at longer lengths scales, including extraction of the produced H_2 from the electrolyte and

exchange of ions between the anode and the cathode. An ion conducting, gas separating membrane is often placed between the electrodes to prevent gas crossover, i.e. the transport of H_2 to the anode or O_2 to the cathode, which could lead to their recombination consuming part of the produced H_2 thereby decreasing the overall system efficiency [163]. The most common materials used for this purpose are porous materials, such as fibrous asbestos and glass frits[59] and ion conductive membranes, such as Nafion[59]. An ideal separator would have low permeability for both H_2 and O_2, while providing high ionic conductivity, however, a compromise between these properties needs to be often made in practice. For example, using a thinner or more porous separator membrane would reduce ohmic losses from the ionic conduction though it, but at the same time increase the crossover rate of the gases[59,163].

Modeling can help optimize separator membranes with respect to these conflicting properties. Transport in porous materials can be modeled with computational fluid dynamics when convection plays a role[59], whereas models based on diffusion and migration alone may suffice to describe transport in denser membranes like Nafion where convection does not occur[59,164]. The separator membrane has already been included, mainly as ohmic losses, in some of the device models presented in the literature[26,59]. Also the effects of the separator properties on H_2 collection efficiency have been studied[163], but detailed models of the effects of the operating conditions on the separator properties (e.g.[164–166]) have not been considered.

6. Device Models

Physical device models combine the individual models of different physical phenomena together in a common geometrical description of the device. Device models have been recently introduced and applied to both single PE [63] and tandem configurations [26,59] as well as to water vapor

electrolysis[167]. They have been also used to study the effect of daily and seasonal variation in the solar irradiation on the hydrogen production, and the effects of temperature [26,168]. They have also demonstrated their usefulness in device level optimization[26,59,163].

Typically, some aspects of device operation are emphasized over the others by describing them theoretically in more detail than the other parts of the model. Such focus points include charge transport in the PE[63,67], mass transport in the electrolyte[16,59], thickness of the catalyst layers[19] or the optical properties of the PE[23]. When the focus has not been on the PE, its operation has often been reduced to BV or similar semi-empirical analytical expression[16,19,59,163]. Detailed PE models have been published as a part of a device model only recently[21,63]. Of the published models the integrated 1D model by Berger and Newman[21] is a remarkable example, because it contains a detailed description of all aspects of the device operation from light absorption to mass transport and homogeneous reactions in the electrolyte. A common approach has been to focus only on the PE and neglect the other device components completely[60,67,89]. In contrast to this, models more focused on electrolyte transport have understandably described the device geometry at much higher level of detail to enable the study of the effect of a wide range of device configurations on the solar-to-hydrogen conversion efficiency while keeping the PE model generic and simple [26,59,167].

There are also practical limitations to which models can be coupled together. For example, it is straightforward to introduce relatively simple analytical kinetic models, such as those of Equation 10 or 11, to a differential equation model of charge carrier generation and transport (Equation 6) so that both are solved together with either analytical or numerical methods. However, whenever the models to be linked follow different mathematical formalism and/or need to be solved with different numerical techniques, they often need to be solved separately. For example, the rate

constants of interfacial reactions could be determined first by DFT calculations, and thereafter used as an input for a device model via Equations 10 or 11. This is appropriate as long as the DFT derived rate constants do not depend significantly on the other variables solved in the device model, such as charge carrier density (Fermi level), the electrostatic potential and surface concentration of the electrolyte species.

A device model can be relatively simple and still give important insight to the optimization of the device. A good example of this is the study about the optical and electrical effects of different catalyst materials on PE performance by Trotochaud et al.[19]. Catalysts are usually considered only for their electrochemical performance and stability. However, since the solar water splitting devices utilize light to drive the reactions, also the optical properties of the catalysts are a real concern[19,169]. It can happen that the electrode with the best catalytic properties may not be the best choice, if the catalyst blocks too much of the incident light. Trotochaud et al. used B-L absorption to model the optical absorption by the catalyst layers, a modified Tafel-equation for the kinetics of the catalyst layers and a diode equation for the current-voltage behavior of the PE. These three models were coupled together to describe the combined effects of the catalyst on the PE performance (Figure 6). The optimal thickness of the studied catalyst materials varied from less than 1 nm to almost 10 nm, depending on the catalytic and optical properties of the material in question[19]. Overall, light absorption was the limiting factor for the catalyst thickness: The materials with the highest absorption coefficients gave the best performance with the thinnest layers, whereas more transparent materials could be utilized as thicker layers[19]. Although a more detailed model might have given more accurate results, this simple model was sufficient to describe the conflict between light absorption and catalytic properties.

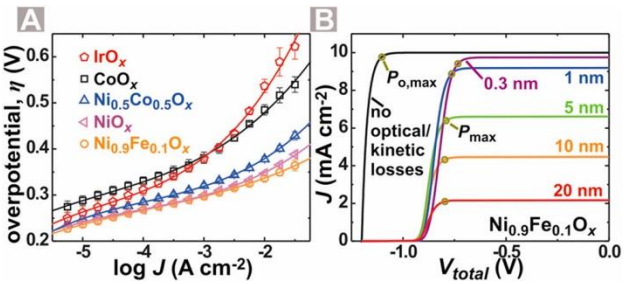

Figure 6. A: Electrokinetic data of studied catalyst materials (points) and polynomial fits to data (lines) B: PE IV-curves calculated for $Ni_{0.9}Fe_{0.1}O_x$ catalyst. Potential axis is versus OER potential ($E(O_2/OH^-) \equiv 0$ V). Reprinted with permission from Ref.[19]. Copyright 2013 American Chemical Society.

A good example of using detailed optical models as a part of device modeling is the study of Dotan et al.[23], who coupled interference effects of the optical generation with a charge transport model. More generally however, demand for detailed optical models might be limited until the overall geometry of the reactors[16,59] and the materials of all their components become more established. Before that, a generic simplified optical model for PE might be sufficient for guiding PE performance optimization.

Similarly to detailed optical modeling, also first principles calculations are rarely, if ever, utilized in device models. As discussed in the previous sections, it is already possible to use them to calculate the energy levels of semiconductors[14], electron[114] and hole mobilities[112], recombination rates[116–118], optical properties[81,82] and reaction rates at different interfaces[141]. It therefore appears that a significant portion of the material properties could already be calculated from the first principles.

DFT calculations have already been used for material screening for promising candidates for water splitting [170,171]. These calculations mainly rely on the stability of the materials in aqueous solutions

and their CB and VB levels although recently estimates for the kinetic overpotentials were also included in the results[171]. These properties reveal both the promising materials and materials that almost certainly would not be useful. Depending on how easy material synthesis and experimental characterization are, and on how accurate and easy simulations are, also device models could be used similarly to further study the applicability of the materials, and how their properties would affect device operation and efficiency.

7. Conclusion

We discussed how physical phenomena are linked with each other and how it is considered in the mathematical modeling of complete PEC devices. This includes both the modeling methods for a particular phenomenon and the approximations made when coupling the phenomena together. We also saw how the device architecture and the geometrical features of the photoelectrodes played a role in the PEC modeling.

The development of computational capacity has increased the level of detail of models and thus also device simulations. This has resulted in increasingly accurate simulations about both the physical phenomena and device geometry although not yet both in the same simulation. The device models have already been used for studies about gas separation and device geometry that would have been difficult to realize with experimental methods. The first principles studies about for example catalyst optimization and the effects of the atom-scale surface structure, also give the same impression of calculating something that cannot be measured. However, although the first principles methods can reliably find the best materials from a number of candidates, the absolute accuracy of their results is not quite as impressive.

In the end, the usefulness of a model does not depend as much on what it can describe as on how it is used. As long as computational capacity does not allow simulating the full operation of the device from the first principles, some simplifications must be made. The efficient utilization of the models therefore depends on both the simulated phenomena and the simplifications in their description, and most importantly on how accurate and computationally heavy the models are. Overall, computational studies are the most useful for phenomena that can be modeled and simulated more accurately than they could be measured. For the first principles modeling of microscopic properties and processes this highlights the attention to the fine details of the physical interactions, as well as to the choice of computational techniques, whereas for the accurate description of the PEC cell operation at the macroscopic scale, multiphysics and multiscale models offer the flexibility needed to mathematically account for the interactions of a broad range of different physical phenomena. The literature covered here shows increasing interest in the modeling of complete PEC devices, which we expect to only intensify as the models and computational methods are further developed and the field moves towards larger device prototypes and systems.

Acknowledgements

This research was funded by Nordic Energy Research (project Nordic Initiative for Solar Fuel Development).

References

(1) Grätzel, M. Photoelectrochemical Cells. *Nature* **2001**, *414*, 338–344.

(2) Guerrero-Lemus, R.; Martínez-Duart, J. M. *Renewable Energies and CO2*; Lecture Notes in Energy; Springer London, 2013.

(3) Acar, C.; Dincer, I. Comparative Assessment of Hydrogen Production Methods from Renewable and Non-Renewable Sources. *Int. J. Hydrogen Energy* **2014**, *39*, 1–12.

(4) Ewan, B.; Allen, R. A Figure of Merit Assessment of the Routes to Hydrogen. *Int. J. Hydrogen Energy* **2005**, *30*, 809–819.

(5) Spath, P. L.; Mann, M. K. *Life Cycle Assessment of Hydrogen Production via Natural Gas Steam Reforming Life Cycle Assessment of Hydrogen Production via Natural Gas Steam Reforming*; Golden, 2001.

(6) Walter, M.; Warren, E. L.; McKone, J. R.; Boettcher, S. W.; Mi, Q.; Santori, E. A.; Lewis, N. S. Solar Water Splitting Cells. *Chem. Rev.* **2010**, *110*, 6446–6473.

(7) Jacobsson, T. J.; Fjällström, V.; Edoff, M.; Edvinsson, T. Sustainable Solar Hydrogen Production: From Photoelectrochemical Cells to PV-Electrolyzers and Back Again. *Energy Environ. Sci.* **2014**, *7*, 2056–2070.

(8) Pinaud, B. A.; Benck, J. D.; Seitz, L. C.; Forman, A. J.; Chen, Z.; Deutsch, T. G.; James, B. D.; Baum, K. N.; Baum, G. N.; Ardo, S.; et al. Technical and Economic Feasibility of Centralized Facilities for Solar Hydrogen Production via Photocatalysis and Photoelectrochemistry. *Energy Environ. Sci.* **2013**, *6*, 1983–2002.

(9) Rocheleau, R. E.; Miller, E. L.; Misra, A. High-Efficiency Photoelectrochemical Hydrogen Production Using Multijunction Amorphous Silicon Photoelectrodes. *Energy & Fuels* **1998**, *0624*, 3–10.

(10) Khaselev, O.; Turner, J. A. A Monolithic Photovoltaic-Photoelectrochemical Device for Hydrogen Production via Water Splitting. *Science* **1998**, *280*, 425–427.

(11) Khaselev, O.; Bansal, A.; Turner, J. A. High-Efficiency Integrated Multijunction Photovoltaic/electrolysis Systems for Hydrogen Production. *Int. J. Hydrogen Energy* **2001**, *26*, 127–132.

(12) Jacobsson, T. J.; Fjällström, V.; Sahlberg, M.; Edoff, M.; Edvinsson, T. A Monolithic Device for Solar Water Splitting Based on Series Interconnected Thin Film Absorbers Reaching over 10% Solar-to-Hydrogen Efficiency. *Energy Environ. Sci.* **2013**, *6*, 3676–3683.

(13) Luo, J.; Im, J.-H.; Mayer, M. T.; Schreier, M.; Nazeeruddin, M. K.; Park, N.-G.; Tilley, S. D.; Fan, H. J.; Grätzel, M. Water Photolysis at 12.3% Efficiency via Perovskite Photovoltaics and Earth-Abundant Catalysts. *Science* **2014**, *345*, 1593–1596.

(14) Calle-Vallejo, F.; Koper, M. T. M. First-Principles Computational Electrochemistry: Achievements and Challenges. *Electrochim. Acta* **2012**, *84*, 3–11.

(15) Liao, P.; Carter, E. A. New Concepts and Modeling Strategies to Design and Evaluate Photo-Electro-Catalysts Based on Transition Metal Oxides. *Chem. Soc. Rev.* **2013**, *42*, 2401–2422.

(16) Carver, C.; Ulissi, Z.; Ong, C. K.; Dennison, S.; Kelsall, G. H.; Hellgardt, K. Modelling and Development of Photoelectrochemical Reactor for H2 Production. *Int. J. Hydrogen Energy* **2012**, *37*, 2911–2923.

(17) Gärtner, W. W. Depletion-Layer Photoeffects in Semiconductors. *Phys. Rev.* **1959**, *116*, 84–87.

(18) Reichman, J. The Current-Voltage Characteristics of Semiconductor-Electrolyte Junction Photovoltaic Cells. *Appl. Phys. Lett.* **1980**, *36*, 574–577.

(19) Trotochaud, L.; Mills, T. J.; Boettcher, S. W. An Optocatalytic Model for Semiconductor–Catalyst Water-Splitting Photoelectrodes Based on In Situ Optical Measurements on Operational Catalysts. *J. Phys. Chem. Lett.* **2013**, *4*, 931–935.

(20) Mills, T. J.; Lin, F.; Boettcher, S. W. Theory and Simulations of Electrocatalyst-Coated Semiconductor Electrodes for Solar Water Splitting. *Phys. Rev. Lett.* **2014**, *112*, 148304.

(21) Berger, A.; Newman, J. An Integrated 1-Dimensional Model of a Photoelectrochemical Cell for Water Splitting. *J. Electrochem. Soc.* **2014**, *161*, E3328–E3340.

(22) Warren, S. C.; Thimsen, E. Plasmonic Solar Water Splitting. *Energy Environ. Sci.* **2012**, *5*, 5133–5146.

(23) Dotan, H.; Kfir, O.; Sharlin, E.; Blank, O.; Gross, M.; Dumchin, I.; Ankonina, G.; Rothschild, A. Resonant Light Trapping in Ultrathin Films for Water Splitting. *Nat. Mater.* **2013**, *12*, 158–164.

(24) Nielander, A. C.; Shaner, M. R.; Papadantonakis, K. M.; Francis, S. A.; Lewis, N. S. A Taxonomy for Solar Fuels Generators. *Energy Environ. Sci.* **2015**, *8*, 16–25.

(25) Peharz, G.; Dimroth, F.; Wittstadt, U. Solar Hydrogen Production by Water Splitting with a Conversion Efficiency of 18%. *Int. J. Hydrogen Energy* **2007**, *32*, 3248–3252.

(26) Haussener, S.; Hu, S.; Xiang, C.; Weber, A. Z.; Lewis, N. S. Simulations of the Irradiation and Temperature Dependence of the Efficiency of Tandem Photoelectrochemical Water-Splitting Systems. *Energy Environ. Sci.* **2013**, *6*, 3604–3618.

(27) Fujishima, A.; Honda, K. Electrochemical Photolysis of Water at a Semiconductor Electrode. *Nature* **1972**, *238*, 37–38.

(28) Shaner, M. R.; Fountaine, K. T.; Ardo, S.; Coridan, R. H.; Atwater, H. A.; Lewis, N. S. Photoelectrochemistry of Core–shell Tandem Junction N–p+-Si/n-WO3 Microwire Array Photoelectrodes. *Energy Environ. Sci.* **2014**, *7*, 779–790.

(29) Habisreutinger, S. N.; Leijtens, T.; Eperon, G. E.; Stranks, S. D.; Nicholas, R. J.; Snaith, H. J. Carbon Nanotube/polymer Composites as a Highly Stable Hole Collection Layer in Perovskite Solar Cells. *Nano Lett.* **2014**, *14*, 5561–5568.

(30) Rau, S.; Vierrath, S.; Ohlmann, J.; Fallisch, A.; Lackner, D.; Dimroth, F.; Smolinka, T. Highly Efficient Solar Hydrogen Generation-An Integrated Concept Joining III-V Solar Cells with PEM Electrolysis Cells. *Energy Technol.* **2014**, *2*, 43–53.

(31) Warren, E. L.; McKone, J. R.; Atwater, H. A.; Gray, H. B.; Lewis, N. S. Hydrogen-Evolution Characteristics of Ni-Mo-Coated, Radial Junction, N+p-Silicon Microwire Array Photocathodes. *Energy Environ. Sci.* **2012**, *5*, 9653–9661.

(32) Cesar, I.; Sivula, K.; Kay, A.; Zboril, R.; Grätzel, M. Influence of Feature Size, Film Thickness, and Silicon Doping on the Performance of Nanostructured Hematite Photoanodes for Solar Water Splitting. *J. Phys. Chem. C* **2009**, *113*, 772–782.

(33) Altermatt, P. P. Models for Numerical Device Simulations of Crystalline Silicon Solar Cells—a Review. *J. Comput. Electron.* **2011**, *10*, 314–330.

(34) Klahr, B. M.; Gimenez, S.; Fabregat-Santiago, F.; Bisquert, J.; Hamann, T. W. Electrochemical and Photoelectrochemical Investigation of Water Oxidation with Hematite Electrodes. *Energy Environ. Sci.* **2012**, *5*, 7626–7636.

(35) Klahr, B. M.; Gimenez, S.; Fabregat-Santiago, F.; Bisquert, J.; Hamann, T. W. Photoelectrochemical and Impedance Spectroscopic Investigation of Water Oxidation with "Co−Pi"-Coated Hematite Electrodes. *J. Am. Chem. Soc.* **2012**, *134*, 16693–16700.

(36) Lopes, T.; Andrade, L.; Le Formal, F.; Grätzel, M.; Sivula, K.; Mendes, A. Hematite Photoelectrodes for Water Splitting: Evaluation of the Role of Film Thickness by Impedance Spectroscopy. *Phys. Chem. Chem. Phys.* **2014**, *16*, 16515–16523.

(37) Kayes, B. M.; Atwater, H. A.; Lewis, N. S. Comparison of the Device Physics Principles of Planar and Radial P-N Junction Nanorod Solar Cells. *J. Appl. Phys.* **2005**, *97*, 114302.

(38) Kelzenberg, M. D.; Boettcher, S. W.; Petykiewicz, J. A.; Turner-Evans, D. B.; Putnam, M. C.; Warren, E. L.; Spurgeon, J. M.; Briggs, R. M.; Lewis, N. S.; Atwater, H. A. Enhanced Absorption and Carrier Collection in Si Wire Arrays for Photovoltaic Applications. *Nat. Mater.* **2010**, *9*, 239–244.

(39) Mann, S. A.; Garnett, E. C. Extreme Light Absorption in Thin Semiconducting Films Wrapped around Metal Nanowires. *Nano Lett.* **2013**, *13*, 3173–3178.

(40) Coridan, R. H.; Arpin, K. A.; Brunschwig, B. S.; Braun, P. V; Lewis, N. S. Photoelectrochemical Behavior of Hierarchically Structured Si/WO3 Core-Shell Tandem Photoanodes. *Nano Lett.* **2014**, *14*, 2310–2317.

(41) Xiang, C.; Meng, A. M.; Lewis, N. S. Evaluation and Optimization of Mass Transport of Redox Species in Silicon Microwire-Array Photoelectrodes. *Proc. Natl. Acad. Sci. U. S. A.* **2012**, *109*, 15622–15627.

(42) Maiolo, J. R.; Kayes, B. M.; Filler, M. A.; Putnam, M. C.; Kelzenberg, M. D.; Atwater, H. A.; Lewis, N. S. High Aspect Ratio Silicon Wire Array Photoelectrochemical Cells. *J. Am. Chem. Soc.* **2007**, *129*, 12346–12347.

(43) Kelzenberg, M. D.; Turner-Evans, D. B.; Putnam, M. C.; Boettcher, S. W.; Briggs, R. M.; Baek, J. Y.; Lewis, N. S.; Atwater, H. A. High-Performance Si Microwire Photovoltaics. *Energy Environ. Sci.* **2011**, *4*, 866.

(44) Hagedorn, K.; Forgacs, C.; Collins, S.; Maldonado, S. Design Considerations for Nanowire Heterojunctions in Solar Energy Conversion/Storage Applications. *J. Phys. Chem. C* **2010**, *114*, 12010–12017.

(45) Zanuccoli, M.; Semenihin, I.; Michallon, J.; Sangiorgi, E.; Fiegna, C. Advanced Electro-Optical Simulation of Nanowire-Based Solar Cells. *J. Comput. Electron.* **2013**, *12*, 572–584.

(46) Strandwitz, N. C.; Turner-Evans, D. B.; Tamboli, A. C.; Chen, C. T.; Atwater, H. A.; Lewis, N. S. Photoelectrochemical Behavior of Planar and Microwire-Array Si|GaP Electrodes. *Adv. Energy Mater.* **2012**, *2*, 1109–1116.

(47) Warren, E. L.; Atwater, H. A.; Lewis, N. S. Silicon Microwire Arrays for Solar Energy-Conversion Applications. *J. Phys. Chem. C* **2014**, *118*, 747–759.

(48) Mohapatra, S. K.; John, S. E.; Banerjee, S.; Misra, M. Water Photooxidation by Smooth and Ultrathin A-Fe2O3 Nanotube Arrays. *Chem. Mater.* **2009**, *21*, 3048–3055.

(49) Cheng, W.; He, J.; Sun, Z.; Peng, Y.; Yao, T.; Liu, Q.; Jiang, Y.; Hu, F.; Xie, Z.; He, B.; et al. Ni-Doped Overlayer Hematite Nanotube: A Highly Photoactive Architecture for Utilization of Visible Light. *J. Phys. Chem. C* **2012**, *116*, 24060–24067.

(50) He, H.; Liu, C.; Dubois, K. D.; Jin, T.; Louis, M. E.; Li, G. Enhanced Charge Separation in Nanostructured TiO2 Materials for Photocatalytic and Photovoltaic Applications. *Ind. Eng. Chem. Res.* **2012**, *51*, 11841–11849.

(51) Cesar, I.; Kay, A.; Gonzalez Martinez, J. A.; Grätzel, M. Translucent Thin Film Fe2O3 Photoanodes for Efficient Water Splitting by Sunlight: Nanostructure-Directing Effect of Si-Doping. *J. Am. Chem. Soc.* **2006**, *128*, 4582–4583.

(52) Warren, S. C.; Voïtchovsky, K.; Dotan, H.; Leroy, C. M.; Cornuz, M.; Stellacci, F.; Hébert, C.; Rothschild, A.; Grätzel, M. Identifying Champion Nanostructures for Solar Water-Splitting. *Nat. Mater.* **2013**, *12*, 842–849.

(53) Danaei, D.; Saeidi, R.; Dabirian, A. Light Trapping in Hematite-Coated Transparent Particles for Solar Fuel Generation. *RSC Adv.* **2015**, *5*, 11946–11951.

(54) Anta, J. A. Electron Transport in Nanostructured Metal-Oxide Semiconductors . *Curr. Opin. Colloid Interface Sci.* **2012**, *17*, 124–131.

(55) De Carvalho, V. A. N.; de S. Luz, R. A.; Lima, B. H.; Crespilho, F. N.; Leite, E. R.; Souza, F. L. Highly Oriented Hematite Nanorods Arrays for Photoelectrochemical Water Splitting. *J. Power Sources* **2012**, *205*, 525–529.

(56) Seger, B.; Pedersen, T.; Laursen, A. B.; Vesborg, P. C. K. K.; Hansen, O.; Chorkendorff, I. Using TiO2 as a Conductive Protective Layer for Photocathodic H2 Evolution. *J. Am. Chem. Soc.* **2013**, *135*, 1057–1064.

(57) Bolton, J. R.; Strickler, S. J.; Connolly, J. S. Limiting and Realizable Efficiencies of Solar Photolysis of Water. *Nature* **1985**, *316*, 495–500.

(58) Hu, S.; Xiang, C.; Haussener, S.; Berger, A. D.; Lewis, N. S. An Analysis of the Optimal Band Gaps of Light Absorbers in Integrated Tandem Photoelectrochemical Water-Splitting Systems. *Energy Environ. Sci.* **2013**, *6*, 2984–2993.

(59) Haussener, S.; Xiang, C.; Spurgeon, J. M.; Ardo, S.; Lewis, N. S.; Weber, A. Z. Modeling, Simulation, and Design Criteria for Photoelectrochemical Water-Splitting Systems. *Energy Environ. Sci.* **2012**, *5*, 9922–9935.

(60) Mora-Seró, I.; Villarreal, T. L.; Bisquert, J.; Pitarch, Á.; Gómez, R.; Salvador, P. Photoelectrochemical Behavior of Nanostructured TiO2 Thin-Film Electrodes in Contact with Aqueous Electrolytes Containing Dissolved Pollutants: A Model for Distinguishing between Direct and Indirect Interfacial Hole Transfer from Photocurrent Measurements. *J. Phys. Chem. B* **2005**, *109*, 3371–3380.

(61) Döscher, H.; Geisz, J.; Deutsch, T.; Turner, J. A. Sunlight Absorption in Water – Efficiency and Design Implications for Photoelectrochemical Devices. *Energy Environ. Sci.* **2014**, *7*, 2951–2956.

(62) Bae, D.; Pedersen, T.; Seger, B. J.; Malizia, M.; Kuznetsov, A.; Hansen, O.; Chorkendorff, I.; Vesborg, P. C. K. Back-Illuminated Si Photocathode: A Combined Experimental and Theoretical Study for Photocatalytic Hydrogen Evolution. *Energy Environ. Sci.* **2015**, *8*, 650–660.

(63) Andrade, L.; Lopes, T.; Ribeiro, H. A.; Mendes, A. Transient Phenomenological Modeling of Photoelectrochemical Cells for Water Splitting - Application to Undoped Hematite Electrodes. *Int. J. Hydrogen Energy* **2011**, *36*, 175–188.

(64) Södergren, S.; Hagfeldt, A.; Olsson, J.; Lindquist, S.-E. Theoretical Models for the Action Spectrum and the Current-Voltage Characteristics of Microporous Semiconductor Films in Photoelectrochemical Cells. *J. Phys. Chem.* **1994**, *98*, 5552–5556.

(65) Liu, B.; Nakata, K.; Liu, S.; Sakai, M.; Ochiai, T.; Murakami, T.; Takagi, K.; Fujishima, A. Theoretical Kinetic Analysis of Heterogeneous Photocatalysis by TiO2 Nanotube Arrays: The Effects of Nanotube Geometry on Photocatalytic Activity. *J. Phys. Chem. C* **2012**, *116*, 7471–7479.

(66) Villarreal, T. L.; Gómez, R.; Neumann-Spallart, M.; Alonso-Vante, N.; Salvador, P. Semiconductor Photooxidation of Pollutants Dissolved in Water: A Kinetic Model for Distinguishing between Direct and Indirect Interfacial Hole Transfer. I. Photoelectrochemical Experiments with Polycrystalline Anatase Electrodes under Current Doubling and. *J. Phys. Chem. B* **2004**, *108*, 15172–15181.

(67) Park, H. S.; Ha, H.-W.; Ruoff, R. S.; Bard, A. J. On the Improvement of Photoelectrochemical Performance and Finite Element Analysis of Reduced Graphene oxide–BiVO4 Composite Electrodes. *J. Electroanal. Chem.* **2014**, *716*, 8–15.

(68) Halme, J.; Vahermaa, P.; Miettunen, K.; Lund, P. Device Physics of Dye Solar Cells. *Adv. Energy Mater.* **2010**, *22*, E210–E234.

(69) Nielsen, M. G.; In, S.-I.; Vesborg, P. C. K.; Pedersen, T.; Almtoft, K. P.; Andersen, I. H.; Hansen, O.; Chorkendorff, I. A Generic Model for Photocatalytic Activity as a Function of Catalyst Thickness. *J. Catal.* **2012**, *289*, 62–72.

(70) Halme, J.; Miettunen, K.; Lund, P. Effect of Nonuniform Generation and Inefficient Collection of Electrons on the Dynamic Photocurrent and Photovoltage Response of Nanostructured Photoelectrodes. *J. Phys. Chem. C* **2008**, *112*, 20491–20504.

(71) Barnes, P. R. F.; Anderson, A. Y.; Durrant, J. R.; O'Regan, B. C. Simulation and Measurement of Complete Dye Sensitised Solar Cells: Including the Influence of Trapping, Electrolyte, Oxidised Dyes and Light Intensity on Steady State and Transient Device Behaviour. *Phys. Chem. Chem. Phys.* **2011**, *13*, 5798–5816.

(72) Luque-Raigon, J. M.; Halme, J.; Miguez, H.; Lozano, G. Symmetry Analysis of the Numerical Instabilities in the Transfer Matrix Method. *J. Opt.* **2013**, *15*, 125719.

(73) Luque-Raigon, J. M.; Halme, J.; Miguez, H. Fully Stable Numerical Calculations for Finite One-Dimensional Structures: Mapping the Transfer Matrix Method. *J. Quant. Spectrosc. Radiat. Transf.* **2014**, *134*, 9–20.

(74) Katsidis, C. C.; Siapkas, D. I. General Transfer-Matrix Method for Optical Multilayer Systems with Coherent, Partially Coherent, and Incoherent Interference. *Appl. Opt.* **2002**, *41*, 3978–3987.

(75) Jäger, K.; Fischer, M.; Van Swaaij, R. A. C. M. M.; Zeman, M. A Scattering Model for Nano-Textured Interfaces and Its Application in Opto-Electrical Simulations of Thin-Film Silicon Solar Cells. *J. Appl. Phys.* **2012**, *111*, 083108.

(76) Gálvez, F. E.; Barnes, P. R. F.; Halme, J.; Miguez, H. Dye Sensitized Solar Cells as Optically Random Photovoltaic Media. *Energy Environ. Sci.* **2014**, *7*, 689–697.

(77) Gálvez, F. E.; Kemppainen, E.; Míguez, H.; Halme, J. Effect of Diffuse Light Scattering Designs on the Efficiency of Dye Solar Cells: An Integral Optical and Electrical Description. *J. Phys. Chem. C* **2012**, *116*, 11426–11433.

(78) Maheu, B.; Letoulouzan, J. N.; Gouesbet, G. Four-Flux Models to Solve the Scattering Transfer Equation in Terms of Lorenz-Mie Parameters. *Appl. Opt.* **1984**, *23*, 3353–3362.

(79) Maheu, B.; Gouesbet, G. Four-Flux Models to Solve the Scattering Transfer Equation: Special Cases. *Appl. Opt.* **1986**, *25*, 1122.

(80) Lin, Y.; Ma, Y. T.; Yang, L.; Xiao, X. R.; Zhou, X. W.; Li, X. P. Computer Simulations of Light Scattering and Mass Transport of Dye-Sensitized Nanocrystalline Solar Cells. *J. Electroanal. Chem.* **2006**, *588*, 51–58.

(81) Ping, Y.; Rocca, D.; Galli, G. Electronic Excitations in Light Absorbers for Photoelectrochemical Energy Conversion: First Principles Calculations Based on Many Body Perturbation Theory. *Chem. Soc. Rev.* **2013**, *42*, 2437–2469.

(82) Noffsinger, J.; Kioupakis, E.; Van de Walle, C. G.; Louie, S. G.; Cohen, M. L. Phonon-Assisted Optical Absorption in Silicon from First Principles. *Phys. Rev. Lett.* **2012**, *108*, 167402.

(83) Ping, Y.; Rocca, D.; Galli, G. Optical Properties of Tungsten Trioxide from First-Principles Calculations. *Phys. Rev. B* **2013**, *87*, 165203.

(84) Nelson, J. *The Physics of Solar Cells*; Imperial College Press, 2003.

(85) Würfel, P. *Physics of Solar Cells: From Basic Principles to Advanced Concepts*, 2nd ed.; John Wiley & Sons, 2009.

(86) Leng, W. H.; Barnes, P. R. F.; Juozapavicius, M.; O'Regan, B. C.; Durrant, J. R. Electron Diffusion Length in Mesoporous Nanocrystalline TiO2 Photoelectrodes during Water Oxidation. *J. Phys. Chem. Lett.* **2010**, *1*, 967–972.

(87) Zhang, Z.; Yates, J. T. Band Bending in Semiconductors: Chemical and Physical Consequences at Surfaces and Interfaces. *Chem. Rev.* **2012**, *112*, 5520–5551.

(88) Phelps, G. J. Calculation of the Internal Electric Field within Doped Semiconductors. *Semicond. Sci. Technol.* **2012**, *27*, 35013.

(89) Bertoluzzi, L.; Bisquert, J. Equivalent Circuit of Electrons and Holes in Thin Semiconductor Films for Photoelectrochemical Water Splitting Applications. *J. Phys. Chem. Lett.* **2012**, *3*, 2517–2522.

(90) Cummings, C. Y.; Marken, F.; Peter, L. M.; Tahir, A. A.; Wijayantha, K. G. U. Kinetics and Mechanism of Light-Driven Oxygen Evolution at Thin Film A-Fe2O3 Electrodes. *Chem. Commun.* **2012**, *48*, 2027–2029.

(91) Peter, L. M. Energetics and Kinetics of Light-Driven Oxygen Evolution at Semiconductor Electrodes: The Example of Hematite. *J. Solid State Electrochem.* **2012**, *17*, 315–326.

(92) Peter, L. M.; Wijayantha, K. G. U.; Tahir, A. A. Kinetics of Light-Driven Oxygen Evolution at A-Fe2O3 Electrodes. *Faraday Discuss.* **2012**, *155*, 309–322.

(93) Liu, B.; Nakata, K.; Zhao, X.; Ochiai, T.; Murakami, T.; Fujishima, A. Theoretical Kinetic Analysis of Heterogeneous Photocatalysis: The Effects of Surface Trapping and Bulk Recombination through Defects. *J. Phys. Chem. C* **2011**, *115*, 16037–16042.

(94) Liu, B.; Zhao, X. A Kinetic Model for Evaluating the Dependence of the Quantum Yield of Nano-TiO2 Based Photocatalysis on Light Intensity, Grain Size, Carrier Lifetime, and Minority Carrier Diffusion Coefficient: Indirect Interfacial Charge Transfer. *Electrochim. Acta* **2010**, *55*, 4062–4070.

(95) Santori, E. A.; Strandwitz, N. C.; Grimm, R. L.; Brunschwig, B. S.; Atwater, H. A.; Lewis, N. S. Operation of Lightly Doped Si Microwires under High-Level Injection Conditions. *Energy Environ. Sci.* **2014**, *7*, 2329.

(96) Foley, J. M.; Price, M. J.; Feldblyum, J. I.; Maldonado, S. Analysis of the Operation of Thin Nanowire Photoelectrodes for Solar Energy Conversion. *Energy Environ. Sci.* **2012**, *5*, 5203–5220.

(97) Anta, J. A. Random Walk Numerical Simulation for Solar Cell Applications. *Energy Environ. Sci.* **2009**, *2*, 387–392.

(98) Cummings, C. Y.; Marken, F.; Peter, L. M.; Wijayantha, K. G. U.; Tahir, A. A. New Insights into Water Splitting at Mesoporous a-Fe2O3 Films: A Study by Modulated Transmittance and Impedance Spectroscopies. *J. Am. Chem. Soc.* **2012**, *134*, 1228–1234.

(99) Le Formal, F.; Sivula, K.; Grätzel, M. The Transient Photocurrent and Photovoltage Behavior of a Hematite Photoanode under Working Conditions and the Influence of Surface Treatments. *J. Phys. Chem. C* **2012**, *116*, 26707–26720.

(100) Gonzalez-Vazquez, J. P.; Anta, J. A.; Bisquert, J. Random Walk Numerical Simulation for Hopping Transport at Finite Carrier Concentrations: Diffusion Coefficient and Transport Energy Concept. *Phys. Chem. Chem. Phys.* **2009**, *11*, 10359–10367.

(101) Nunzi, F.; Mosconi, E.; Storchi, L.; Ronca, E.; Selloni, A.; Grätzel, M.; De Angelis, F. Inherent Electronic Trap States in TiO2 Nanocrystals: Effect of Saturation and Sintering. *Energy Environ. Sci.* **2013**, *6*, 1221–1229.

(102) Kopidakis, N.; Neale, N. R.; Zhu, K.; van de Lagemaat, J.; Frank, A. J. Spatial Location of Transport-Limiting Traps in TiO2 Nanoparticle Films in Dye-Sensitized Solar Cells. *Appl. Phys. Lett.* **2005**, *87*, 202106.

(103) Mercado, C.; Knorr, F. Location of Hole and Electron Traps on Nanocrystalline Anatase TiO2. *J. Phys. Chem. C* **2012**, *116*, 10796–10804.

(104) Gonzalez-Vazquez, J.; Morales-Flórez, V.; Anta, J. A. How Important Is Working with an Ordered Electrode to Improve the Charge Collection Efficiency in Nanostructured Solar Cells? *J. Phys. Chem. Lett.* **2012**, *3*, 386–393.

(105) Ansari-Rad, M.; Anta, J. A.; Bisquert, J. Interpretation of Diffusion and Recombination in Nanostructured and Energy Disordered Materials by Stochastic Quasiequilibrium Simulation. *J. Phys. Chem. C* **2013**, *117*, 16275–16289.

(106) Huda, M. N.; Al-Jassim, M. M.; Turner, J. A. Mott Insulators: An Early Selection Criterion for Materials for Photoelectrochemical H2 Production. *J. Renew. Sustain. Energy* **2011**, *3*, 053101.

(107) Vo, T.; Williamson, A. J.; Galli, G. First Principles Simulations of the Structural and Electronic Properties of Silicon Nanowires. *Phys. Rev. B* **2006**, *74*, 045116.

(108) Xu, X.; Randorn, C.; Efstathiou, P.; Irvine, J. T. S. A Red Metallic Oxide Photocatalyst. *Nat. Mater.* **2012**, *11*, 595–598.

(109) Ouyang, S.; Ye, J. B-AgAl1-xGaxO2 Solid-Solution Photocatalysts: Continuous Modulation of Electronic Structure toward High-Performance Visible-Light Photoactivity. *J. Am. Chem. Soc.* **2011**, *133*, 7757–7763.

(110) Iordanova, N.; Dupuis, M.; Rosso, K. M. Theoretical Characterization of Charge Transport in Chromia (α-Cr2O3). *J. Chem. Phys.* **2005**, *123*, 074710.

(111) Deskins, N. A.; Dupuis, M. Electron Transport via Polaron Hopping in Bulk TiO2: A Density Functional Theory Characterization. *Phys. Rev. B* **2007**, *75*, 195212.

(112) Liao, P.; Carter, E. A. Hole Transport in Pure and Doped Hematite. *J. Appl. Phys.* **2012**, *112*, 13701.

(113) Iordanova, N.; Dupuis, M.; Rosso, K. M. Charge Transport in Metal Oxides: A Theoretical Study of Hematite A-Fe2O3. *J. Chem. Phys.* **2005**, *122*, 144305.

(114) Liao, P.; Toroker, M. C.; Carter, E. A. Electron Transport in Pure and Doped Hematite. *Nano Lett.* **2011**, *11*, 1775–1781.

(115) Varshney, D.; Yogi, A. Structural and Electrical Conductivity of Mn Doped Hematite (α-Fe2O3) Phase. *J. Mol. Struct.* **2011**, *995*, 157–162.

(116) Steiauf, D.; Kioupakis, E.; Van de Walle, C. G. Auger Recombination in GaAs from First Principles. *ACS Photonics* **2014**, *1*, 643–646.

(117) Delaney, K. T.; Rinke, P.; Van de Walle, C. G. Auger Recombination Rates in Nitrides from First Principles. *Appl. Phys. Lett.* **2009**, *94*, 191109.

(118) Krishnamurthy, S.; Berding, M. A. Full-Band-Structure Calculation of Shockley–Read–Hall Recombination Rates in InAs. *J. Appl. Phys.* **2001**, *90*, 848.

(119) Bard, A. J.; Faulkner, L. R. *Electrochemical Methods: Fundamentals and Applications*; WILEY-VCH Verlag, 2001.

(120) Durst, J.; Siebel, A.; Simon, C.; Hasché, F.; Herranz, J.; Gasteiger, H. A. New Insights into the Electrochemical Hydrogen Oxidation and Evolution Reaction Mechanism. *Energy Environ. Sci.* **2014**, *7*, 2255–2260.

(121) Sheng, W.; Gasteiger, H. A.; Shao-Horn, Y. Hydrogen Oxidation and Evolution Reaction Kinetics on Platinum: Acid vs Alkaline Electrolytes. *J. Electrochem. Soc.* **2010**, *157*, B1529.

(122) Neyerlin, K. C.; Gu, W.; Jorne, J.; Gasteiger, H. A. Study of the Exchange Current Density for the Hydrogen Oxidation and Evolution Reactions. *J. Electrochem. Soc.* **2007**, *154*, B631–B635.

(123) Chen, S.; Kucernak, A. R. Electrocatalysis under Conditions of High Mass Transport: Investigation of Hydrogen Oxidation on Single Submicron Pt Particles Supported on Carbon. *J. Phys. Chem. B* **2004**, *108*, 13984–13994.

(124) Wang, J. X.; Springer, T. E.; Liu, P.; Shao, M.; Adzic, R. R. Hydrogen Oxidation Reaction on Pt in Acidic Media: Adsorption Isotherm and Activation Free Energies. *J. Phys. Chem. C* **2007**, *111*, 12425–12433.

(125) Wang, J. X.; Springer, T. E.; Adzic, R. R. Dual-Pathway Kinetic Equation for the Hydrogen Oxidation Reaction on Pt Electrodes. *J. Electrochem. Soc.* **2006**, *153*, A1732–A1740.

(126) Harrison, J.; Khan, Z. The Oxidation of Hydrogen. *J. Electroanal. Chem. Interfacial Electrochem.* **1971**, *30*, 327–330.

(127) Durst, J.; Simon, C.; Gasteiger, H. A. Hydrogen Oxidation and Evolution Reaction Kinetics on Carbon Supported Pt , Ir , Rh , and Pd Electrocatalysts in Acidic Media. *J. Electrochem. Soc.* **2015**, *162*, F190–F203.

(128) Rheinländer, P. J.; Herranz, J.; Durst, J.; Gasteiger, H. A. Kinetics of the Hydrogen Oxidation/Evolution Reaction on Polycrystalline Platinum in Alkaline Electrolyte Reaction Order with Respect to Hydrogen Pressure. *J. Electrochem. Soc.* **2014**, *161*, F1448–F1457.

(129) Gerischer, H.; Heller, A. The Role of Oxygen in Photooxidation of Organic Molecules on Semiconductor Particles. *J. Phys. Chem.* **1991**, *95*, 5261–5267.

(130) Khan, S. U. M.; Bockris, J. O. A Model for Electron Transfer at the Illuminated P-Type Semiconductor-Solution Interface. *J. Phys. Chem.* **1984**, *88*, 2504–2515.

(131) Shreve, G. A.; Lewis, N. S. An Analytical Description of the Consequences of Abandoning the Principles of Detailed Balance and Microscopic Reversibility in Semiconductor Photoelectrochemistry. *J. Electrochem. Soc.* **1995**, *142*, 112–119.

(132) Lin, F.; Boettcher, S. W. Adaptive Semiconductor/electrocatalyst Junctions in Water-Splitting Photoanodes. *Nat. Mater.* **2013**, *13*, 81–86.

(133) Sousa, C.; Tosoni, S.; Illas, F. Theoretical Approaches to Excited-State-Related Phenomena in Oxide Surfaces. *Chem. Rev.* **2013**, *113*, 4456–4495.

(134) Valdés, Á.; Brillet, J.; Grätzel, M.; Gudmundsdóttir, H.; Hansen, H. A.; Jónsson, H.; Klüpfel, P.; Kroes, G.-J.; Le Formal, F.; Man, I. C.; et al. Solar Hydrogen Production with Semiconductor Metal Oxides: New Directions in Experiment and Theory. *Phys. Chem. Chem. Phys.* **2012**, *14*, 49–70.

(135) Pilania, G.; Ramprasad, R. Dielectric Permittivity of Ultrathin PbTiO3 Nanowires from First Principles. *J. Mater. Sci.* **2012**, *47*, 7580–7586.

(136) Rossmeisl, J.; Skúlason, E.; Björketun, M. E.; Tripkovic, V.; Nørskov, J. K. Modeling the Electrified Solid–liquid Interface. *Chem. Phys. Lett.* **2008**, *466*, 68–71.

(137) Koper, M. T. M. Thermodynamic Theory of Multi-Electron Transfer Reactions: Implications for Electrocatalysis . *J. Electroanal. Chem.* **2011**, *660*, 254–260.

(138) Rossmeisl, J.; Logadottir, A.; Nørskov, J. K. Electrolysis of Water on (oxidized) Metal Surfaces. *Chem. Phys.* **2005**, *319*, 178–184.

(139) Rossmeisl, J.; Nørskov, J. K.; Taylor, C. D.; Janik, M. J.; Neurock, M. Calculated Phase Diagrams for the Electrochemical Oxidation and Reduction of Water over Pt(111). *J. Phys. Chem. B* **2006**, *110*, 21833–21839.

(140) Nørskov, J. K.; Bligaard, T.; Rossmeisl, J.; Christensen, C. H. Towards the Computational Design of Solid Catalysts. *Nat. Chem.* **2009**, *1*, 37–46.

(141) Keith, J. A.; Jacob, T. Theoretical Studies of Potential-Dependent and Competing Mechanisms of the Electrocatalytic Oxygen Reduction Reaction on Pt(111). *Angew. Chemie Int. Ed.* **2010**, *49*, 9521–9525.

(142) Keith, J. A.; Jerkiewicz, G.; Jacob, T. Theoretical Investigations of the Oxygen Reduction Reaction on Pt(111). *ChemPhysChem* **2010**, *11*, 2779–2794.

(143) Shen, X.; Small, Y.; Wang, J. Photocatalytic Water Oxidation at the GaN $(10\bar{1}0)-$ Water Interface. *J. Phys. Chem. C* **2010**, *114*, 13695–13704.

(144) Valdés, Á.; Kroes, G.-J. First Principles Study of the Photo-Oxidation of Water on Tungsten Trioxide (WO3). *J. Chem. Phys.* **2009**, *130*, 114701.

(145) Nørskov, J. K.; Bligaard, T.; Hvolbaek, B.; Abild-Pedersen, F.; Chorkendorff, I.; Christensen, C. H. The Nature of the Active Site in Heterogeneous Metal Catalysis. *Chem. Soc. Rev.* **2008**, *37*, 2163–2171.

(146) Jackson, A.; Viswanathan, V.; Forman, A. J.; Larsen, A. H.; Nørskov, J. K.; Jaramillo, T. F. Climbing the Activity Volcano: Core-Shell Ru@Pt Electrocatalysts for Oxygen Reduction. *ChemElectroChem* **2014**, *1*, 67–71.

(147) Vojvodic, A.; Medford, A. J.; Studt, F.; Abild-Pedersen, F.; Khan, T. S.; Bligaard, T.; Nørskov, J. K. Exploring the Limits: A Low-Pressure, Low-Temperature Haber–Bosch Process. *Chem. Phys. Lett.* **2014**, *598*, 108–112.

(148) Honkala, K.; Hellman, A.; Remediakis, I. N.; Logadottir, A.; Carlsson, A.; Dahl, S.; Christensen, C. H.; Nørskov, J. K. Ammonia Synthesis from First-Principles Calculations. *Science* **2005**, *307*, 555–558.

(149) Lim, D.-H.; Wilcox, J. Mechanisms of the Oxygen Reduction Reaction on Defective Graphene-Supported Pt Nanoparticles from First-Principles. *J. Phys. Chem. C* **2012**, *116*, 3653–3660.

(150) Prodan, E.; Kohn, W. Nearsightedness of Electronic Matter. *Proc. Natl. Acad. Sci. U. S. A.* **2005**, *102*, 11635–11638.

(151) Prodan, E. Nearsightedness of Electronic Matter in One Dimension. *Phys. Rev. B - Condens. Matter Mater. Phys.* **2006**, *73*, 085108.

(152) Tang, W.; Peterson, A. A.; Varela, A. S.; Jovanov, Z. P.; Bech, L.; Durand, W. J.; Dahl, S.; Nørskov, J. K.; Chorkendorff, I. The Importance of Surface Morphology in Controlling the Selectivity of Polycrystalline Copper for CO2 Electroreduction. *Phys. Chem. Chem. Phys.* **2012**, *14*, 76–81.

(153) Schouten, K. J. P.; Kwon, Y.; van der Ham, C. J. M.; Qin, Z.; Koper, M. T. M. A New Mechanism for the Selectivity to C1 and C2 Species in the Electrochemical Reduction of Carbon Dioxide on Copper Electrodes. *Chem. Sci.* **2011**, *2*, 1902–1909.

(154) Medford, A. J.; Lausche, A. C.; Abild-Pedersen, F.; Temel, B.; Schjødt, N. C.; Nørskov, J. K.; Studt, F. Activity and Selectivity Trends in Synthesis Gas Conversion to Higher Alcohols. *Top. Catal.* **2013**, *57*, 135–142.

(155) Trainor, T. P.; Chaka, A. M.; Eng, P. J.; Newville, M.; Waychunas, G. A.; Catalano, J. G.; Brown, G. E. Structure and Reactivity of the Hydrated Hematite (0001) Surface. *Surf. Sci.* **2004**, *573*, 204–224.

(156) Hellman, A.; Pala, R. G. First-Principles Study of Photoinduced Water-Splitting on Fe2O3. *J. Phys. Chem. C* **2011**, *115*, 12901–12907.

(157) Nguyen, M.-T.; Seriani, N.; Piccinin, S.; Gebauer, R. Photo-Driven Oxidation of Water on A-Fe2O3 Surfaces: An Ab Initio Study. *J. Chem. Phys.* **2014**, *140*, 064703.

(158) Liao, P.; Keith, J. A.; Carter, E. A. Water Oxidation on Pure and Doped Hematite (0001) Surfaces: Prediction of Co and Ni as Effective Dopants for Electrocatalysis. *J. Am. Chem. Soc.* **2012**, *134*, 13296–13309.

(159) Barbier, A.; Stierle, A.; Kasper, N.; Guittet, M.-J.; Jupille, J. Surface Termination of Hematite at Environmental Oxygen Pressures: Experimental Surface Phase Diagram. *Phys. Rev. B* **2007**, *75*, 233406.

(160) Kiejna, A.; Pabisiak, T. Mixed Termination of Hematite (α-Fe2O3)(0001) Surface. *J. Phys. Chem. C* **2013**, *117*, 24339–24344.

(161) Medford, A. J.; Wellendorff, J.; Vojvodic, A.; Studt, F.; Abild-Pedersen, F.; Jacobsen, K. W.; Bligaard, T.; Nørskov, J. K. Assessing the Reliability of Calculated Catalytic Ammonia Synthesis Rates. *Science* **2014**, *345*, 197–200.

(162) Akimov, A. V; Muckerman, J. T.; Prezhdo, O. V. Nonadiabatic Dynamics of Positive Charge during Photocatalytic Water Splitting on GaN(10-10) Surface: Charge Localization Governs Splitting Efficiency. *J. Am. Chem. Soc.* **2013**, *135*, 8682–8691.

(163) Berger, A.; Segalman, R. A.; Newman, J. Material Requirements for Membrane Separators in a Water-Splitting Photoelectrochemical Cell. *Energy Environ. Sci.* **2014**, *7*, 1468–1476.

(164) Choi, P.; Jalani, N. H.; Datta, R. Thermodynamics and Proton Transport in Nafion: II. Proton Diffusion Mechanisms and Conductivity. *J. Electrochem. Soc.* **2005**, *152*, E123–E130.

(165) Choi, P.; Jalani, N. H.; Datta, R. Thermodynamics and Proton Transport in Nafion: I. Membrane Swelling, Sorption and Ion-Exchange Equilibrium. *J. Electrochem. Soc.* **2005**, *152*, E84–E89.

(166) Choi, P.; Jalani, N. H.; Datta, R. Thermodynamics and Proton Transport in Nafion: III. Proton Transport in Nafion/Sulfated ZrO2 Nanocomposite Membranes. *J. Electrochem. Soc.* **2005**, *152*, A1548–A1554.

(167) Xiang, C.; Chen, Y.; Lewis, N. S. Modeling an Integrated Photoelectrolysis System Sustained by Water Vapor. *Energy Environ. Sci.* **2013**, *6*, 3713–3721.

(168) Andrade, L.; Lopes, T.; Mendes, A. Dynamic Phenomenological Modeling of Pec Cells for Water Splitting Under Outdoor Conditions. *Energy Procedia* **2012**, *22*, 23–34.

(169) Riha, S. C.; Klahr, B. M.; Tyo, E. C.; Seifert, S.; Vajda, S.; Pellin, M. J.; Hamann, T. W.; Martinson, A. B. F. Atomic Layer Deposition of a Submonolayer Catalyst for the Enhanced Photoelectrochemical Performance of Water Oxidation with Hematite. *ACS Nano* **2013**, *7*, 2396–2405.

(170) Castelli, I. E.; Olsen, T.; Datta, S.; Landis, D. D.; Dahl, S.; Thygesen, K. S.; Jacobsen, K. W. Computational Screening of Perovskite Metal Oxides for Optimal Solar Light Capture. *Energy Environ. Sci.* **2012**, *5*, 5814–5819.

(171) Montoya, J. H.; Garcia-Mota, M.; Nørskov, J. K.; Vojvodic, A. Theoretical Evaluation of the Surface Electrochemistry of Perovskites with Promising Photon Absorption Properties for Solar Water Splitting. *Phys. Chem. Chem. Phys.* **2015**, *17*, 2634–2640.

Table of contents figure

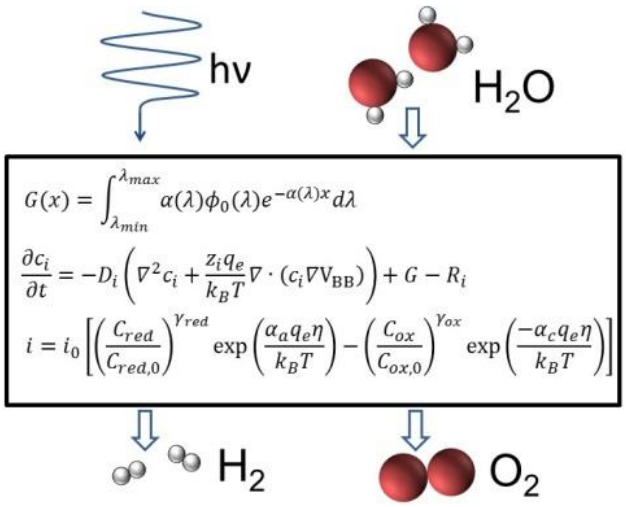

Author biographies

Erno Kemppainen

Erno Kemppainen received his M.Sc. (Tech.) degree in Advanced Energy Systems in 2012 and he is currently a doctoral student in Aalto University School of Science. He has studied dye-sensitized solar cells and his current research is focused on physics-based modeling of photoelectrochemical hydrogen production. His research interests include electrochemistry and conversion and storage of solar energy.

Janne Halme

Janne Halme has D.Sc. (Tech.) degree in engineering physics from Helsinki University of Technology and is currently a University Lecturer at the Aalto University School of Science. He has carried out both fundamental and applied research of dye-sensitized solar cells (DSSC) with a particular focus on flexible printed devices and their advanced performance characterization techniques. His current research interests are in electrochemical energy conversion and storage, building integrated photovoltaics and ambient energy harvesting.

Peter Lund

Peter Lund is a professor in Engineering Physics at the Aalto University School of Science working on future energy questions. He is particularly interested in multidisciplinary approaches in energy. Energy transitions, smart urban energy, and nanoenergy are his current research themes.